Usama Riaz

Comparison of converter control schemes for weak grids

School of Electrical Engineering

Thesis submitted for examination for the degree of Master of Science in Technology.

Espoo 23.04.2018

Thesis supervisor:

Prof. Marko Hinkkanen

Thesis advisor:

F. M. Mahafugur Rahman, M.Sc. (Tech.)

Aalto University
School of Electrical
Engineering

AALTO UNIVERSITY
SCHOOL OF ELECTRICAL ENGINEERING

ABSTRACT OF THE
MASTER'S THESIS

Author: Usama Riaz

Title: Comparison of converter control schemes for weak grids

Date: 23.04.2018 Language: English Number of pages:7+62

Department of Electrical Engineering and Automation

Professorship: Electric Drives Code: ELEC 3024

Supervisor: Prof. Marko Hinkkanen

Advisor: F. M. Mahafugur Rahman, M.Sc. (Tech.)

Voltage source converter is used in power systems for connecting a renewable energy source to an AC grid or as an active front-end rectifiers in AC motor drives. When the conventional control methods (vector control and power-angle control) are used to control a converter that is connected to a weak grid, the performance of the resulting system is degraded. High power demands degrade the quality of the transferred power and can even make the system unstable. A relatively new control scheme known as power-synchronization control is introduced to rectify the problem. The scheme keeps the system stable under weak-grid conditions but the damping for strong grids is compromised. The scheme needs to switch to a back-up vector control during fault conditions. This violates the initial motivation of developing a new control scheme. This thesis identifies the root causes of the stability problems in vector control when connected to weak grids. The state-of-the-art vector control scheme is used as a starting point. The role of the phase-locked loop and AC-voltage controller in the stability of the system is explored. Two novel modifications in the vector control scheme are presented. The converter-voltage reference or the measured converter voltage is used as a feedback to modify the active and reactive power references. The modifications ensure improved performance of vector control for weak grids. Better damping and faster dynamic response are obtained as compared to power-synchronization control and conventional vector control. The benchmark performance of the standard vector control for strong grids is not compromised by these modifications. The dynamic performance and robustness of the control schemes are tested and compared using time domain simulations.

Keywords: Converter-voltage feedback, current control, grid-connected converter, L filter, phase-locked loop, power-synchronization control, short-circuit ratio, vector control, weak grid.

Preface

The research work reported in this thesis has been carried out at Aalto University, Finland in the Department of Automation and Electrical Engineering. The work has been financially supported by ABB Oy as a part of an ongoing research project.

I would like to express my deepest gratitude to my supervisor Prof. Marko Hinkkanen for giving me this wonderful opportunity to work in his research group. I would like to thank him for his advice, guidance, and valuable suggestions regarding my thesis. I also want to thank my instructor F. M. Mahafugur Rahman for his comments, suggestions, and corrections in the scientific writing.

I would like to thank all the people from ABB Oy specially Dr. Mikko Routimo and Prof. Lennart Harnefors for their valuable comments and suggestions during the work. I would like to thank all of my colleagues at the electric drives research group for creating a pleasant working environment. I would also like to thank my friends Abid, Bilal and Faisal for their moral support during the process.

Finally, I would like to express my deepest love and gratitude to my whole family, especially to my parents for their endless support and encouragement throughout my life.

Espoo, 23.04.2018

Usama Riaz

Contents

Symbols and abbreviations

Symbols

Boldface letters represent the vectors. The magnitude of the vectors are denoted by plain italic letters.

C_{dc}	DC-link capacitor
d_{abc}	Duty ratios
$\boldsymbol{e}$	Internal generated voltage of a synchronous machine
$\boldsymbol{e}_{\mathrm{g}}$	Grid voltage
$\boldsymbol{i}_{\mathrm{a}}$	Stator current of a synchronous machine
H	High-pass filter transfer function for modified vector control
H_{hp}	High-pass filter transfer function for PSC
H_{lp}	Low-pass filter transfer function for PCC voltage measurement
$\boldsymbol{i}_{\mathrm{c}}$	Converter current
J	Inertia of a rotor shaft
k_{dc}	DC-link controller gain
k_{ii}	Integral gain of the current controller
k_{pi}	Proportional gain of the current controller
K_{h}	High-pass filter gain
K_{p}	Integral gain of APC
L	Sum of filter and grid inductance
L_{a}	Stator inductance of a synchronous machine
L_{c}	Filter inductance
L_{g}	Grid inductance
L_{t}	Sum of line and stator inductance of a synchronous machine
P	Active power transferred between two systems
P_{dc}	DC-source power
$P_{\mathrm{dc,N}}$	Rated power of the DC bus
q_{abc}	State of converter switches
Q	Reactive power transferred between two systems
r	Active damping resistance of the current controller
R	Active damping resistance of PSC
R_{a}	Stator resistance of a synchronous machine
S_{ac}	Short-circuit power of an AC system
T_{e}	Electromagnetic torque
T_{m}	Mechanical torque on a rotor shaft

u	Converter voltage magnitude in PSC
u_{aN}	Converter pole voltage
$\boldsymbol{u}_{\mathrm{c}}$	Converter voltage
u_{dc}	DC-link voltage
$\boldsymbol{u}_{\mathrm{g}}$	PCC voltage
W_{dc}	Energy stored in the DC bus
Y_{g}	Plant transfer function
α_{c}	Current controller bandwidth
α_{h}	Bandwidth of the high-pass filter H
δ	Phase difference between the converter and the grid voltage
ω_{c}	Low-pass filter bandwidth
ω_{b}	High-pass filter bandwidth
ω_{e}	Nominal electrical angular frequency of a synchronous machine
ω_{m}	Angular frequency of a rotor
ω_{N}	Nominal angular frequency of a grid
ω_{g}	Angular frequency of a grid
$\hat{\omega}_{\mathrm{g}}$	Estimated angular frequency of a grid
ω_{PLL}	Output angular frequency of the PLL in PSC
θ	Phase angle of the converter voltage
θ_{e}	Phase difference between the voltages of a synchronous machine
θ_{g}	Grid voltage angle
$\hat{\theta}_{\mathrm{g}}$	Estimated grid voltage angle

Abbreviations

APC	Active-power controller of PSC
LPF	Low-pass filter
PCC	Point of common coupling
PLL	Phase-locked loop
PWM	Pulse-width modulation
PSC	Power-synchronization control
SCR	Short-circuit ratio
SM	Synchronous machine
VSC	Voltage source converter
VSM	Virtual synchronous machine

1 Introduction

Due to the increased prices, scarcity and environmental affects of fossil fuels, power sector is replacing conventional power plants with renewable energy sources [1]. It is not always cost effective or reliable to transmit power to remote areas from centralized generation units. So, a distributed generation is preferred [2]. Often, a distributed generation is based on renewable energy sources. The use of wind turbines and solar photo-voltaic panels to generate electricity is common nowadays.

The output of a renewable source is usually not feasible to be directly connected to a power grid. Since the output of a solar panel is DC, a DC to AC converter is needed between the panels and the grid. The output frequency of wind turbines varies from time to time due to intermittent nature of wind. The output of a wind turbine is first converted to DC and then to AC of a desired frequency, before connecting it to a grid. A grid converter is used to convert DC to AC or vice verse. The control of this converter is a challenging and developing field.

Voltage source converter (VSC) is a common choice of converter in power systems. There are some challenges in using a converter with a weak AC grid [3], [4]. Wind turbines are usually located in remote areas where the transmission and distribution grids are weak. Also, the major portion of solar photo-voltaic generation is connected at the distribution level where the grids are weak. The weak grid is defined as a grid with the short-circuit ratio (SCR) < 3 according to IEEE standard 1204-1997 [5]. SCR is the ratio of the maximum (short-circuit) apparent power of the grid to the rated power of the interconnecting generator.

There are two basic control schemes used for a VSC: 1) power-angle control [6]; 2) vector current control [7]. Power-angle control is simply a scalar control scheme. The active power is controlled by controlling the phase-angle shift between the grid voltage and the output voltage. The reactive power is controlled by controlling the magnitude of the output voltage. A phase-locked loop (PLL) is needed to synchronize a converter to a grid. There are some disadvantages of using this scheme: 1) it cannot limit the valve current which can trip the converter; 2) a PLL is required which can cause stability issues in weak grids [8].

Vector current control is a popular control scheme for variable speed drives. Due to its successful implementation in motor drives, it is a preferable choice for grid converters. The active and reactive power is controlled using current components. Hence, limiting the current is very easy and inherent. This protects the inverter from tripping due to over-currents under fault conditions. Vector control is able to support the grid under fault conditions.

Vector control does not utilize a VSC to its full potential under weak-grid conditions [22, 24]. If no AC-voltage controller is used, vector-controlled converter can only transfer up to 0.6 p.u of the power for SCR = 1 [9]. Another difficulty in using vector control is that it uses a PLL to estimate the phase angle of the grid voltage. Studies have shown that the PLL affects the performance and stability of the system [8].

To solve the above mentioned problems, many new control schemes have been introduced in the literature [10–12]. Most of these control schemes aim to mimic the operation of a synchronous machine without using a PLL. In [11], one such notable control scheme known as the power-synchronization control has been presented. The mechanical dynamics of a synchronous machine are emulated in the control structure. PSC synchronizes a converter with a grid using an active power transfer technique. So there is no limitation on the SCR of the grid, i.e., a converter can be connected to either a strong or weak grid [13–15].

The PSC scheme is similar to the power-angle control scheme in which the active power is controlled by the phase angle and the reactive power is controlled by adjusting the converter voltage magnitude. The difference is that PSC does not use a PLL to synchronize its output to the grid voltage. So, the stability problems related to the PLL are eliminated. Although other problems such as an over-current protection can also be dealt with, by switching the control from PSC to vector control in the case of faults, it makes the implementation very complex

This thesis analyzes the performance of a converter using two state-of-the-art control schemes, i.e., vector control and PSC. An L filter is used between the converter and the grid to suppress the harmonics generated by the converter. The schemes are tested for strong and weak-grid conditions. The analysis is carried out for a normal grid operation without any fault conditions. The objective of this thesis is to compare and identify the scheme that works best for all grid strengths without re-tuning any controller.

The thesis consists of six sections. Section 2 introduces the grid converter equipped with an L filter. Section 3 introduces and explains the state-of-the-art control schemes for grid converters, problems faced under weak-grid conditions and their solutions. Two novel modified vector control schemes are introduced with the focus on performance in weak grids. Section 4 discusses the tuning and parameters selection of the controllers. Section 5 presents the simulation results of the control schemes introduced in Section 3 and compares them. In Section 6, the thesis is concluded based on the results in Section 5 and probable future extension of the work.

2 Grid Converter With an L Filter

In this section, the basic concepts of the topic are introduced. A system model is presented which is needed for testing the control schemes. The performance of a converter depends on the characteristics of the grid and the type of a filter used with the converter. A brief description of the synchronization in synchronous machines is also discussed at the end.

2.1 System Model

In Fig. 2.1, a two-level three-phase VSC connected to the grid is shown, where u_{dc} is the DC-link voltage and C_{dc} is the DC-link capacitor. A grid converter is a power electronic device which enables bi-directional power flow between the DC bus and the grid.

There are eight combinations of switches. The state of these switches is represented by q. 1 means that the switch is in the upward position and 0 means that it is in the downward position. For example, q_{abc}=101 means that nodes 'a' and 'c' are connected to the positive terminal of the DC bus and node 'b' is connected to the negative terminal (N) of the DC bus.

The three phase output voltages of the converter at any instant can be represented in space vector form as

$$\boldsymbol{u}_{\mathrm{c}}^{s} = \frac{2}{3}(u_{\mathrm{aN}} + u_{\mathrm{bN}}\mathrm{e}^{j\frac{2\pi}{3}} + u_{\mathrm{cN}}\mathrm{e}^{j\frac{4\pi}{3}}) \tag{2.1}$$

where superscript 's' denotes that the voltage is in stationary reference frame and

$$u_{\mathrm{aN}} = q_{\mathrm{a}}u_{\mathrm{dc}} \qquad u_{\mathrm{bN}} = q_{\mathrm{b}}u_{\mathrm{dc}} \qquad u_{\mathrm{cN}} = q_{\mathrm{c}}u_{\mathrm{dc}} \tag{2.2}$$

Eq. (2.1) can also be written as:

$$\boldsymbol{u}_{\mathrm{c}}^{s} = \frac{2}{3}(q_{\mathrm{a}} + q_{\mathrm{b}}\mathrm{e}^{j\frac{2\pi}{3}} + q_{\mathrm{c}}\mathrm{e}^{j\frac{4\pi}{3}})u_{\mathrm{dc}} \tag{2.3}$$

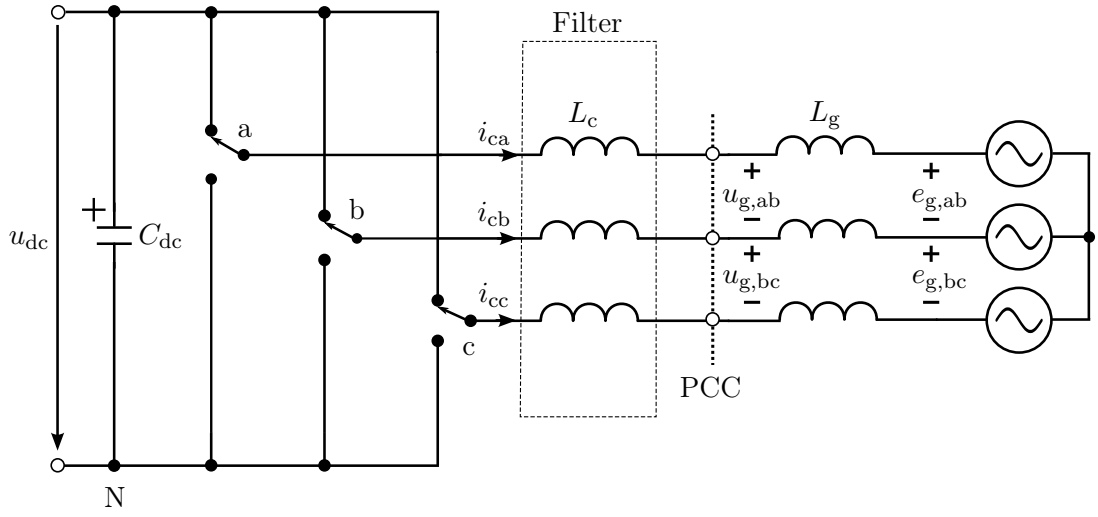

Figure 2.1: Grid converter switch model.

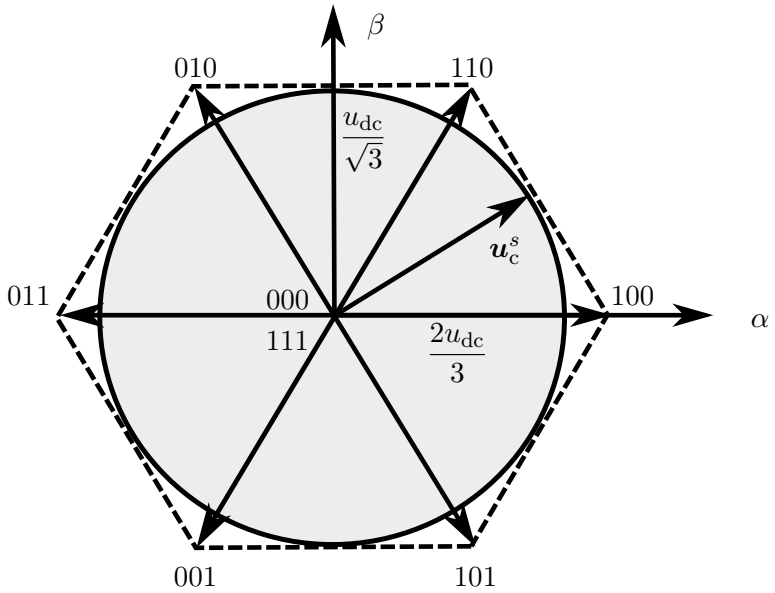

Figure 2.2: Converter space vector in $\alpha\beta$ coordinates.

The graphical representation of the space vector is shown in Fig. 2.2. The hexagon is obtained by inserting different values of q_{abc} which are mentioned along each vector. Two zero vectors and six non zero vectors are obtained.

Using pulse-width modulation (PWM), any voltage vector inside the hexagon can be obtained. Multiple vectors can be used during a switching cycle to obtain the desired averaged voltage vector. The magnitude can be reduced by using zero vectors in between other vectors

$$\overline{\boldsymbol{u}_c^s} = \frac{2}{3}(d_a + d_b e^{j\frac{2\pi}{3}} + d_c e^{j\frac{4\pi}{3}})u_{dc} \tag{2.4}$$

where d_{abc} are the duty ratios ranging $0 \ldots 1$.

The circle inside the hexagon represents the region of linear modulation. The maximum voltage that can be achieved in the linear region is $u_{\mathrm{dc}}/\sqrt{3}$. The maximum voltage that can be achieved in the non-linear region is represented by the corners of the hexagon, i.e., $(2/3)u_{\mathrm{dc}}$. In $\alpha\beta$ coordinates, the vectors rotate with an angular frequency ω_{g}. It is convenient to use Park's transformation (or also known as dq transformation), which is:

$$\boldsymbol{u}_{\mathrm{c}} = \boldsymbol{u}_{\mathrm{c}}^{s} e^{-j\theta_{\mathrm{g}}} \tag{2.5}$$

The dq coordinate system rotates with an angular frequency ω_{g}. The dq coordinate system is also known as synchronous coordinate system. Since the vectors are now stationary in steady state, it is much easier to analyze and design the system.

The converter is connected to the grid at the point of common coupling (PCC). The filter inductance L_{c} is used to reduce the voltage harmonics present in the converter output voltage. The grid inductance L_{g} is the measure of the grid's strength. The power is transferred between the grid and the converter at the PCC.

2.2 L Filter

The output voltage of the converter is a high frequency pulse train. These pulses are the result of the switching, used to generate the desired AC voltage from the DC voltage. The switching frequency of the converter usually ranges from 1 kHz to 20 kHz. Higher harmonics are present at the multiples of the switching frequency. In order to follow the IEEE-519 standard for harmonic distortion [16], it is not possible to connect this output directly to a grid. An L or LCL filter is commonly used between the converter and the grid, in order to remove the converter harmonics and provide smooth sinusoidal currents to the grid. In this thesis, an L filter is used to filter out the harmonics. The merits and demerits of both of these filter types are out of the scope of this work.

2.3 Short-Circuit Ratio

The short-circuit ratio (SCR) is defined as the ratio of the maximum (short circuit) apparent power of the grid to the rated power of the interconnecting generator. The SCR is used to define the strength of the grid. Grids with small SCR are considered weak whereas grids with high SCR are considered stiff. It is still a challenge to design a robust converter control for weak grids. SCR can also be defined in terms of the grid impedance. Grids with high impedance are considered weak whereas grids with low impedance are considered strong or stiff. The weak grid is defined

as a grid with SCR < 3 and the strong grid is defined as the grid with SCR > 5 according to the IEEE standard 1204-1997 [5]. The SCR is

$$\text{SCR} = \frac{S_{\text{ac}}}{P_{\text{dc,N}}} \tag{2.6}$$

where S_{ac} is the short-circuit power of an AC system and $P_{\text{dc,N}}$ is the rated power of the DC bus

$$S_{\text{ac}} = \frac{u_{\text{g}}^2}{\omega_{\text{g}} L_{\text{g}}} \tag{2.7}$$

To simplify the expression, the PCC voltage u_{g} is considered to be the base value of voltage and $P_{\text{dc,N}}$ is considered to be the base value of power. If we represent the impedance in per unit then from (2.6) and (2.7), we get

$$\text{SCR} = \frac{1}{\omega_{\text{g}} L_{\text{g}}} \tag{2.8}$$

since ω_{g} is usually 1 p.u., (2.8) becomes

$$\text{SCR} = \frac{1}{L_{\text{g}}\ [\text{p.u.}]} \tag{2.9}$$

The above equation defines the SCR as it is seen from the PCC. Sometimes, the SCR is also defined as seen from the converter terminals. In that case, L_{g} is replaced by $L = L_{\text{c}} + L_{\text{g}}$. In this thesis, the SCR is defined as seen from the converter terminals, i.e.,

$$\text{SCR} = \frac{1}{L\ [\text{p.u.}]} \tag{2.10}$$

2.4 Virtual Synchronous Machines

Virtual synchronous machine (VSM) is an emerging concept of controlling a grid converter [10–12, 17, 18]. This control scheme emulates the operation of a synchronous machine. The behavior of a synchronous machine can be emulated by implementing a complete model or an approximate model of a synchronous machine. For example, [11] only implements a part of swing equation and leaves out the inertial emulation part whereas, [10] and [12] includes inertia as well. The advantage of this scheme over conventional control methods is that its operation does not depend upon the grid strength. This means that the performance of a control scheme is not compromised when connected to a weak grid. Conventional schemes use a PLL which causes stability issues in weak grids. VSM does not need a PLL to synchronize with the grid. Besides this, VSM can also emulate the inertial characteristics of a synchronous machine. The increasing amount of renewable energy generation in power systems results in the lack of inertia. Inertia plays an important role in the stability of power systems.

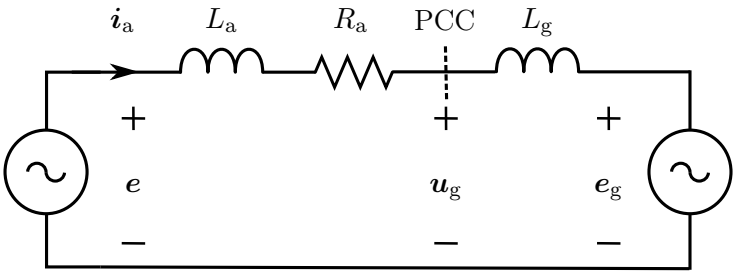

Figure 2.3: Synchronous machine connected to a grid

There are two broad categories of control schemes among VSMs which are discussed as follows

2.4.1 Voltage-Controlled Converters

Fig. 2.3 shows the connection of a synchronous generator to the grid, where $\boldsymbol{e}$ is the internal generated voltage of the synchronous machine , $\boldsymbol{u}_\mathrm{g}$ is the output voltage of the synchronous generator or the PCC voltage, L_a is the stator inductance, R_a is the stator resistance, L_g is the grid inductance and $\boldsymbol{e}_\mathrm{g}$ is the grid voltage. The voltage equation of the synchronous generator can be written in Laplace domain as

$$\boldsymbol{u}_\mathrm{g}(s) = \boldsymbol{e}(s) - (R_\mathrm{a} + sL_\mathrm{a})\boldsymbol{i}_\mathrm{a}(s) \tag{2.11}$$

The above equation can be easily implemented in the control system of a converter to obtain a voltage-controlled VSM. The disadvantages of using this straight forward implementation is that the control system cannot limit over currents. Additional backup schemes are needed to implement over current protection. This can make the implementation complex. This scheme is also known as virtual impedance control [12].

2.4.2 Current-Controlled Converters

This control scheme implements (2.11) in an alternative way as follows

$$\boldsymbol{i}_\mathrm{a}(s) = \frac{1}{R_\mathrm{a} + sL_\mathrm{a}} \left(\boldsymbol{e}\,(s) - \boldsymbol{u}_\mathrm{g}\,(s)\right) \tag{2.12}$$

The above equation determines the stator current of the synchronous machine when the internal generated voltage and the terminal voltage are known. The above equation can be implemented in the control of a converter to obtain the current reference from the reference internal generated voltage and the measured terminal voltage. This current reference is then realized by the fast inner current controller

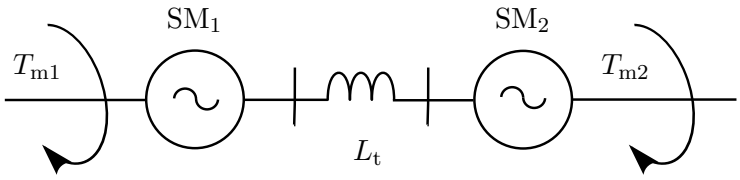

Figure 2.4: Synchronization in synchronous machines.

like in the vector control scheme. The current controller makes it very easy to limit fault currents.

Both the voltage-controlled converters and the current-controlled converters need to emulate the mechanical dynamics of a synchronous machine. In order to implement the mechanical behavior of a synchronous machine, let's first revisit the concept of synchronization and power transfer in synchronous machines.

2.4.3 Power Transfer in Synchronous Machines

Control methods for weak grids are developed to emulate a synchronization mechanism used by synchronous machines (SM). In Fig. 2.4, two synchronous machines are shown which are connected together through an inductance L_t which is the sum of the line inductance and stator inductance of the SM. The model is considered to be loss-less. SM_1 is operating as a generator and SM_2 is operating as a motor. When two SMs are at steady state, then the power transferred from SM_1 to SM_2 is given by

$$P = \frac{e_2 e_1 \sin\theta_\mathrm{e}}{\omega_\mathrm{e} L_\mathrm{t}} \tag{2.13}$$

where e_1 and e_2 are the magnitudes of the internally generated voltages of SM_1 and SM_2 respectively, θ_e is the phase difference between the two voltages and ω_e is the nominal electrical angular frequency of the system. Now assume that the mechanical torque T_m1 on the shaft of SM_1 is increased momentarily. As a result, the mechanical angle of the rotor of SM_1 advances, according to the equation

$$J_1 \frac{d\omega_\mathrm{m1}}{dt} = T_\mathrm{m1} - T_\mathrm{e1} \tag{2.14}$$

where J_1 is the inertia of the rotor shaft of SM_1, ω_m1 is the angular speed of the rotor and T_e1 is the electromagnetic torque of the SM_1. Since the internally generated voltage $\boldsymbol{e_1}$ is tightly coupled with the motion of the rotor shaft, increase in the mechanical angle of the rotor shaft produces phase advancement in the emf $\boldsymbol{e_1}$. The advancement in the phase of $\boldsymbol{e_1}$ increases the phase difference between the two voltages $\boldsymbol{e_1}$ and $\boldsymbol{e_2}$. According to (2.13), the power transfer from SM_1 to SM_2 will increase. This increase in power can also be seen as an increase in the electromagnetic torque T_e2 of SM_2. If the mechanical load T_m2 on the shaft of SM_2 is constant

then the rotor accelerates according to the equation

$$J_2 \frac{d\omega_{\mathrm{m2}}}{dt} = T_{\mathrm{e2}} - T_{\mathrm{m2}} \tag{2.15}$$

where J_2 is the inertia of the rotor shaft of SM_2 and ω_{m2} is the angular speed of the rotor. The increase in the speed of the rotor of SM_2 will produce the same effect as in SM_1, i.e., the phase of voltage $\boldsymbol{e_2}$ advances. This results in the reduction of the phase difference between $\boldsymbol{e_1}$ and $\boldsymbol{e_2}$. The power transferred from e_1 to e_2 is restored to its initial value and the system achieves the steady state again.

The synchronism of a power system is maintained by the transfer of the transient power. This transfer of transient power is the basis of VSMs. Vector control and power-angle control do not use this method for synchronism instead a PLL is used to synchronize with the grid. The power control loop in VSM is based on the same concept as described above. The power is controlled by the phase difference δ between the grid and the converter voltage. The power controller not only controls active power but also synchronizes the converter with the grid. The mechanical dynamics of a SM are implemented in this controller.

3 Control Schemes for VSCs

In this section, the most commonly used control methods for grid converters are discussed. Each scheme will be discussed in detail including the working principle, control structure, advantages and disadvantages. The main focus will be on studying and analyzing the performance of each scheme under weak-grid conditions. At the end, two novel modifications in the vector control scheme are also suggested which improve the performance under weak-grid conditions.

3.1 Standard Vector Control

Vector control is a popular and widely used control method for grid converters [7,19]. After becoming a popular control method for AC motors, vector control was also used to control VSCs [20]. The grid model is analogous to the AC motor model which makes the vector control a viable option. In Fig. 3.1, a simplified circuit diagram of a VSC connected to a grid is shown, where $\boldsymbol{u}_{\mathrm{c}}^{s}$ is the converter voltage, $\boldsymbol{u}_{\mathrm{g}}^{s}$ is the PCC voltage, L_{c} is the filter inductance, L_{g} is the grid inductance and $\boldsymbol{e}_{\mathrm{g}}^{s}$ is the grid voltage. The resistance of the filter and the grid are small as compared to their inductances, so they are neglected in most of the following calculations unless specified otherwise.

Vector control consists of a fast inner current control loop and outer loops. The inner loop is used to control the current based on the current reference generated by the outer loops. The outer loops consist of a DC-link voltage controller and an AC-voltage controller. The choice of outer-loop controllers is application specific. For example, the DC-link controller is used when the converter is required to regulate the voltage of the DC bus. Active power and DC-link voltage cannot be controlled simultaneously by the same converter. Similarly, reactive power and AC voltage cannot be controlled at the same time. Usually, a reactive-power controller is used with strong grids and an AC-voltage controller is used with weak grids. The reason is that the PCC voltage in weak grids is not constant [14] and needs to be regulated. It is a function of current $\boldsymbol{i}_{\mathrm{c}}$.

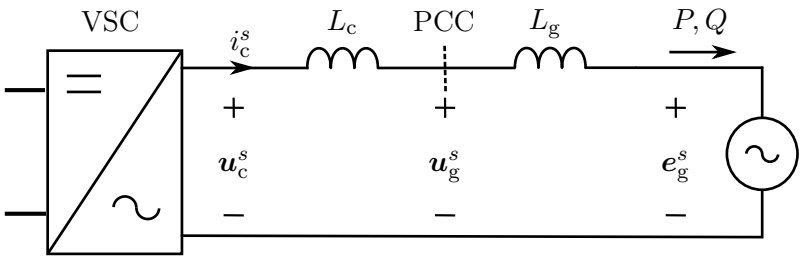

Figure 3.1: Circuit diagram of a grid connected converter.

Vector control technique is based on using a synchronized reference frame revolving at the same frequency as the grid voltage. The advantage of using a synchronous frame is that all the vectors appear static. In vector control, the d-axis of the dq frame is aligned to the PCC voltage. This provides decoupling between the active and reactive power. The voltage equation of the circuit in Fig. 3.1 can be written in synchronous coordinates as

$$-\boldsymbol{u}_\mathrm{c} + L_\mathrm{c}\frac{d\boldsymbol{i}_\mathrm{c}}{dt} + \mathrm{j}\omega_\mathrm{g} L_\mathrm{c}\boldsymbol{i}_\mathrm{c} + \boldsymbol{u}_\mathrm{g} = 0 \tag{3.1}$$

The above vectors can be written in the component form as

$$\boldsymbol{i}_\mathrm{c} = i_\mathrm{cd} + \mathrm{j}i_\mathrm{cq}, \qquad \boldsymbol{u}_\mathrm{c} = u_\mathrm{cd} + \mathrm{j}u_\mathrm{cq}, \qquad \boldsymbol{u}_\mathrm{g} = u_\mathrm{gd} + \mathrm{j}u_\mathrm{gq} \tag{3.2}$$

The active power is given by

$$P = \frac{3}{2}\,\mathrm{Re}\,\{\boldsymbol{u}_\mathrm{g}\boldsymbol{i}_\mathrm{c}^*\} = \frac{3}{2}(u_\mathrm{gd}i_\mathrm{cd} + u_\mathrm{gq}i_\mathrm{cq}) \tag{3.3}$$

and the reactive power is given by

$$Q = \frac{3}{2}\,\mathrm{Im}\,\{\boldsymbol{u}_\mathrm{g}\boldsymbol{i}_\mathrm{c}^*\} = \frac{3}{2}(u_\mathrm{gq}i_\mathrm{cd} - u_\mathrm{gd}i_\mathrm{cq}) \tag{3.4}$$

Since the d-axis is aligned to the PCC voltage, the active and reactive power become

$$P = \frac{3}{2}u_\mathrm{g}i_\mathrm{cd} \qquad\qquad Q = -\frac{3}{2}u_\mathrm{g}i_\mathrm{cq} \tag{3.5}$$

From the above equations, it is visible that the active and reactive power can be controlled separately. The d component of the current controls the active power whereas the q component of the current controls the reactive power.

The vectors in two coordinate systems are shown in Fig. 3.2. The block diagram of vector control is shown in Fig. 3.3. The current reference $\boldsymbol{i}_\mathrm{c,ref}$ is calculated based on (3.5). The inner current controller is a fast proportional-integral (PI) controller

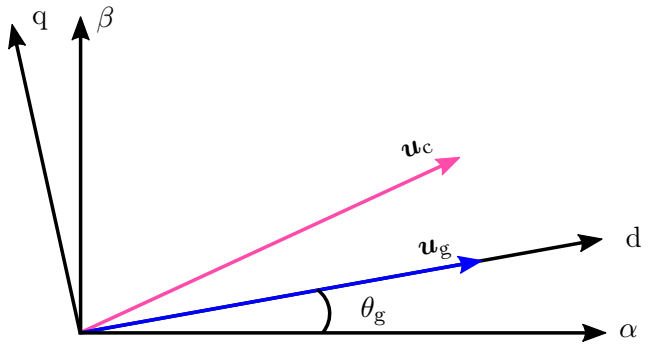

Figure 3.2: Stationary and synchronous coordinates.

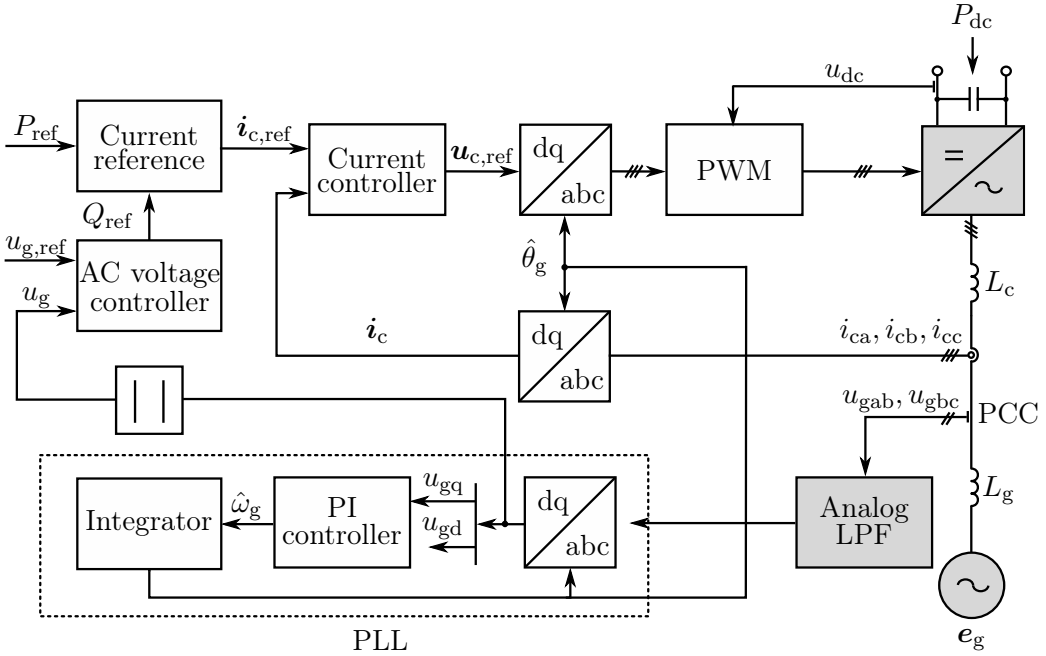

Figure 3.3: Block diagram of standard vector control.

which realizes the current reference generated by the outer-loop controllers. The design parameters of these controllers will be discussed in Section 4.

3.1.1 Phase-Locked Loop

In order to synchronize the converter with the grid, a PLL is used [21]. It tracks the phase angle of the PCC voltage and synchronizes the converter based on this angle. The phase angle cannot be used directly as it is noisy. The PLL reduces the noise above its bandwidth and uses a PI controller to eliminate the steady state error.

A PI controller is used whose input is u_{gq} which is treated as an error signal and is driven to 0. The output of the PI controller is the estimated grid frequency. This

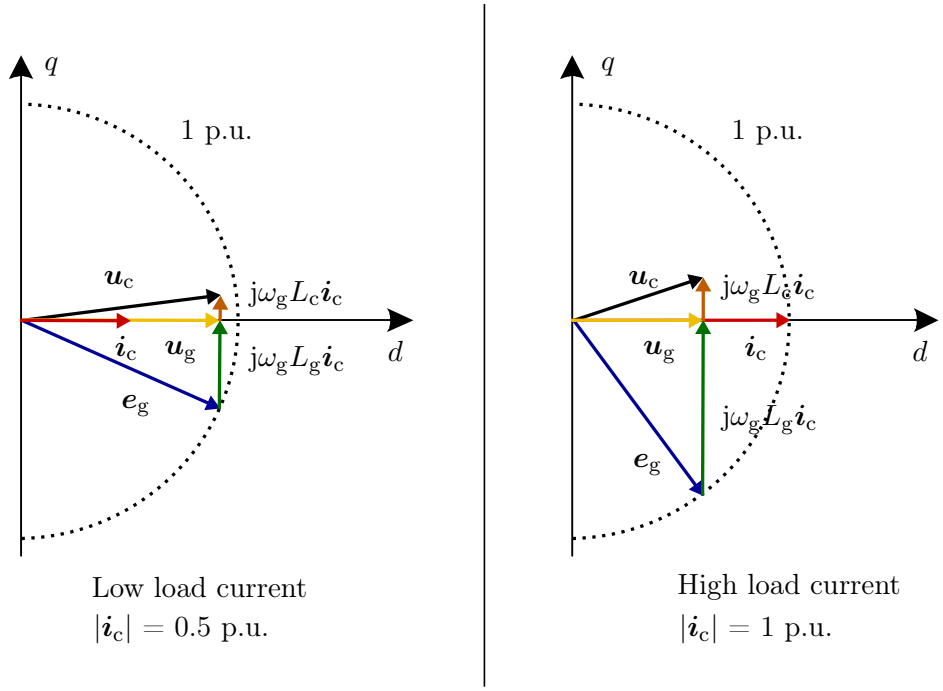

Figure 3.4: Vector diagram.

frequency is further integrated to get an estimated PCC voltage phase angle.

When the vector control scheme is used to control the converter connected to a weak grid, the resulting system may become unstable or poorly damped [22]. The PCC voltage in weak grids is not stiff [23]. It varies with the variations in the converter current. A fast PLL response makes the system very sensitive to the changes in the PCC voltage. The operation of a VSC in weak grids is analyzed in more details in the following sections.

3.1.2 Weak Grid and Vector Control Limitations

The vector control scheme shows fast dynamic response when used to control a converter connected to a strong grid. However, it is still a challenge to connect the converter to a very weak grid (SCR < 2) [3, 4, 11, 15, 17, 18, 22]. The grid inductance in weak grids is large as compared to the filter inductance. Due to this reason, PCC voltage $\boldsymbol{u}_g$ varies with the variations in the converter current $\boldsymbol{i}_c$

A vector-controlled grid converter cannot transfer 1 p.u. of active power in weak grids due to the PCC voltage collapse. The magnitude of the PCC voltage depends on the magnitude of the converter current. The magnitude of the converter current depends on the power reference. In Fig. 3.4, two vector diagrams are shown to illustrates the operation of a vector-controlled converter connected to a weak grid. The q component of current is assumed to be zero. Two operating points are chosen to show the dependency of the PCC voltage on the converter current. It can be

clearly seen that for high load current (1 p.u.), the PCC voltage has reduced as compared to low load current (0.5 p.u.). Although the phase angle between the converter and the grid voltage increases with the power reference, the active power cannot be increased beyond 0.6 p.u. for SCR =1. In order to transfer 1 p.u. of active power, the reactive power should be supplied to the grid. An AC-voltage controller is needed to regulate the PCC voltage to 1 p.u. This is posible by the transfer of reactive power. In theory, it might be possible to regulate the PCC voltage to 1 p.u. to transfer 1 p.u. of active power but in reality the converter current ratings should also be considered [22]

There are multiple sources of problems for the instability of vector-controlled converter connected to a weak grid. Some of them are: 1) outer-loop controllers 2) fast PLL response (High PLL bandwidth)

In order to transfer 1 p.u. of power between a converter and a weak grid while maintaining stability, many new converter control schemes have been introduced in the literature [10–12, 17, 18, 24]. Some of the schemes are discussed in the following sections.

3.2 PCC Voltage Measurement

Before discussing in detail about the different schemes used for weak grids, the problem of measuring the PCC voltage $\boldsymbol{u}_{\mathrm{g}}$ should be addressed. In weak grids, the filter impedance is smaller than the grid impedance. As a result, the PCC voltage contains the PWM ripple of the converter voltage.

The measured PCC voltage is used by the PLL and the AC-voltage controller. The control system cannot work properly with the PWM ripple of the converter in the PCC voltage. In order to obtain the fundamental component of the PCC voltage, an analog Low-pass filter (LPF) is used.

The drawback of using the LPF is that it introduces gain and phase errors in the filtered output. The gain and phase errors can be calculated. The bandwidth of the low-pass filter is represented by ω_{c}. The transfer function of a first-order LPF can be written in Laplace domain as

$$H_{\mathrm{lp}}(s) = \frac{\omega_{\mathrm{c}}}{s + \omega_{\mathrm{c}}} \tag{3.6}$$

In frequency domain

$$H_{\mathrm{lp}}(j\omega_{\mathrm{g}}) = \frac{\omega_{\mathrm{c}}}{j\omega_{\mathrm{g}} + \omega_{\mathrm{c}}} \tag{3.7}$$

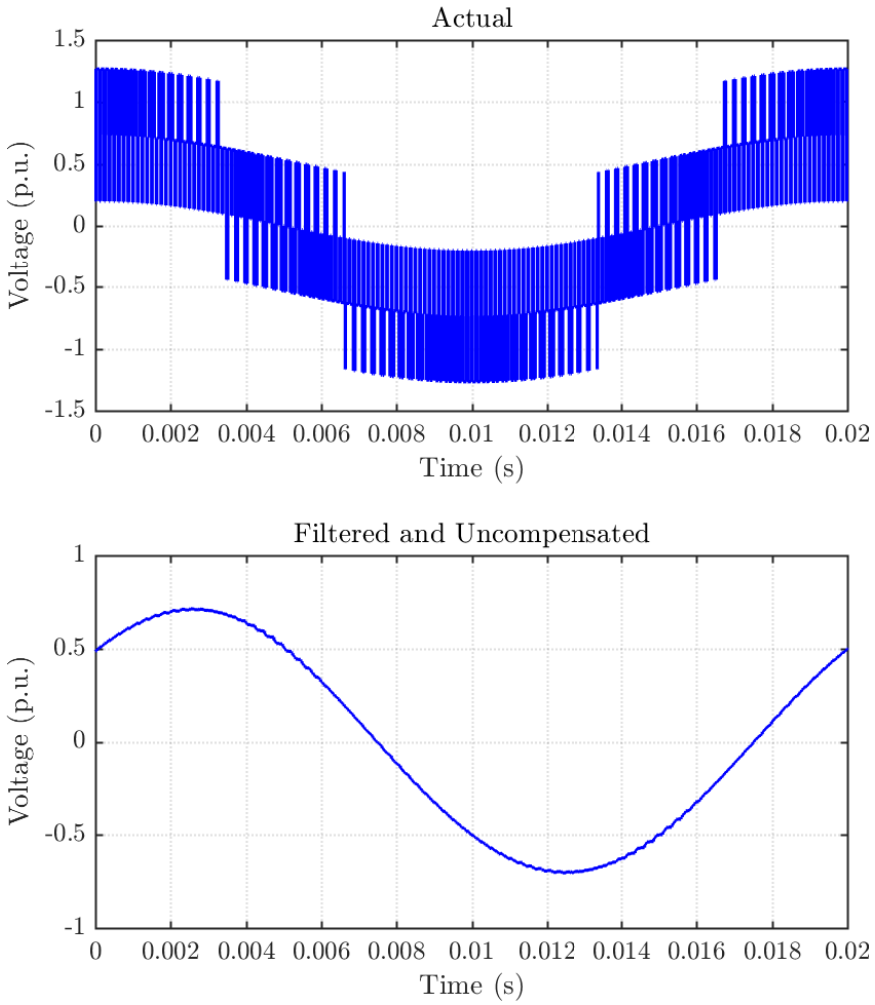

Figure 3.5: Actual vs filtered PCC voltage.

The gain and phase of the LPF as the function of the input frequency are

$$|H_{\mathrm{lp}}(j\omega_{\mathrm{g}})| = \sqrt{\frac{\omega_{\mathrm{c}}^2}{\omega_{\mathrm{g}}^2 + \omega_{\mathrm{c}}^2}} \quad ; \quad \angle H_{\mathrm{lp}}(j\omega_{\mathrm{g}}) = -\arctan\left(\frac{\omega_{\mathrm{g}}}{\omega_{\mathrm{c}}}\right) \tag{3.8}$$

The above expressions for gain and phase of the LPF shows that the LPF introduces errors in the gain and phase of the input. The error in the phase and gain of the filtered PCC voltage can be compensated for in the control system. In this thesis, ω_{c} is selected to be equal to the nominal angular frequency ω_{N}.

3.3 Power-Synchronization Control

The power-synchronization control (PSC) is a converter control scheme invented to solve the problem of connecting a converter to a very weak grid. It was first

introduced in [11, 13]. PSC works on the principle of transient power transfer in synchronous machines as discussed in Section 2.4.3. PSC falls under the category of voltage-controlled VSM discussed in Section 2.4.1 which means that there is no inner current controller. PSC does not need the PLL under normal operation. Therefore, the performance and stability issues due to the PLL in weak grids are eliminated. Another difference between vector control and PSC is that the converter voltage magnitude is kept constant in PSC. The active power is controlled by adjusting the phase angle of the converter voltage. Conversely, in vector control, the converter voltage varies in order to regulate the converter current to a reference value calculated from the active and reactive power references. The performance of PSC does not depend on the PCC voltage. The PSC-controlled converter can transfer 1 p.u. of active power without regulating the PCC voltage magnitude to 1 p.u. Though, the PCC voltage magnitude can still be regulated by adjusting the converter voltage magnitude. PSC works for a wide range of SCR without the need of re-tuning any controller.

3.3.1 Control Principle of PSC

The control law of PSC is based on the transfer of transient power like in synchronous machines. This transient power is used to maintain synchronism with the grid. The active power is transferred by adjusting the phase angle of the converter voltage

$$\frac{d\delta}{dt} = K_{\mathrm{p}}(P_{\mathrm{ref}} - P) \tag{3.9}$$

where δ is the phase difference between the converter and the grid voltage, P_{ref} is the reference value of the active power which can be adjusted manually or through an outer-loop DC-link voltage controller. The value of δ changes corresponding to the change in the reference power. K_{p} is the integral gain of the active-power controller. The active power P at the converter terminals is calculated as

$$P = \frac{3}{2}\,\mathrm{Re}\,\{\boldsymbol{u}_{\mathrm{c}}\boldsymbol{i}_{\mathrm{c}}^{*}\} \tag{3.10}$$

In PSC, the d-axis of the dq reference frame is aligned to the converter voltage

$$P = \frac{3}{2}\,u_{\mathrm{c}}i_{\mathrm{cd}} \tag{3.11}$$

The converter voltage in PSC can be selected as

$$\boldsymbol{u}_{\mathrm{c,ref}}^{s} = ue^{\mathrm{j}\theta} \tag{3.12}$$

$$\theta = \omega_{\mathrm{N}}t + \delta \tag{3.13}$$

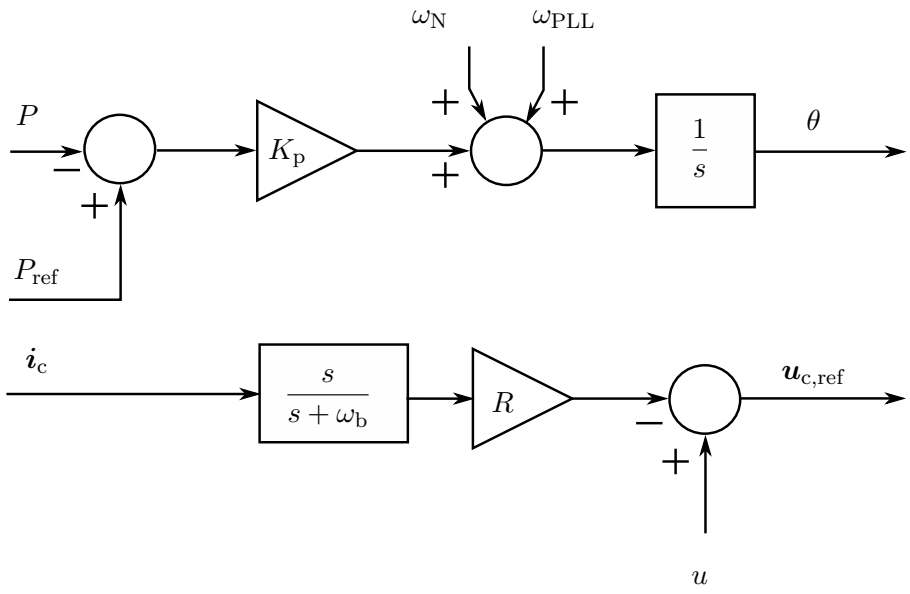

Figure 3.6: PSC control law.

where θ is the phase angle of the converter voltage, ω_{N} is the nominal angular frequency and u is the converter voltage magnitude normally selected to be 1 p.u. or controlled by an outer-loop AC-voltage controller or a reactive-power controller. The converter voltage magnitude can also be controlled in such a way that it emulates the droop characteristic of the exciter of a synchronous machine.

3.3.2 Active Damping

The converter voltage reference in (3.12) cannot be used directly because it results in a poorly damped system. The solution is to use the concept of active damping [11, 25]. An active damping resistance is a virtual resistance implemented in the control system, used to damp the oscillations in the current and power. A high-pass filtered converter current with the gain R is subtracted from the converter voltage magnitude. The converter reference voltage becomes

$$\boldsymbol{u}_{\mathrm{c,ref}} = u - R \cdot H_{\mathrm{hp}} \boldsymbol{i}_{\mathrm{c}} \tag{3.14}$$

where R is the active damping resistance and H_{hp} is the high-pass filter

$$\boldsymbol{u}_{\mathrm{c,ref}} = u - R \frac{s}{s+\omega_{\mathrm{b}}} \boldsymbol{i}_{\mathrm{c}} \tag{3.15}$$

The filter bandwidth ω_{b} should be selected smaller than ω_{N}, i.e., $0.2\omega_{\mathrm{N}}$ or 0.2 p.u. and R is also selected to have similar value, i.e., 0.2 p.u. [26]

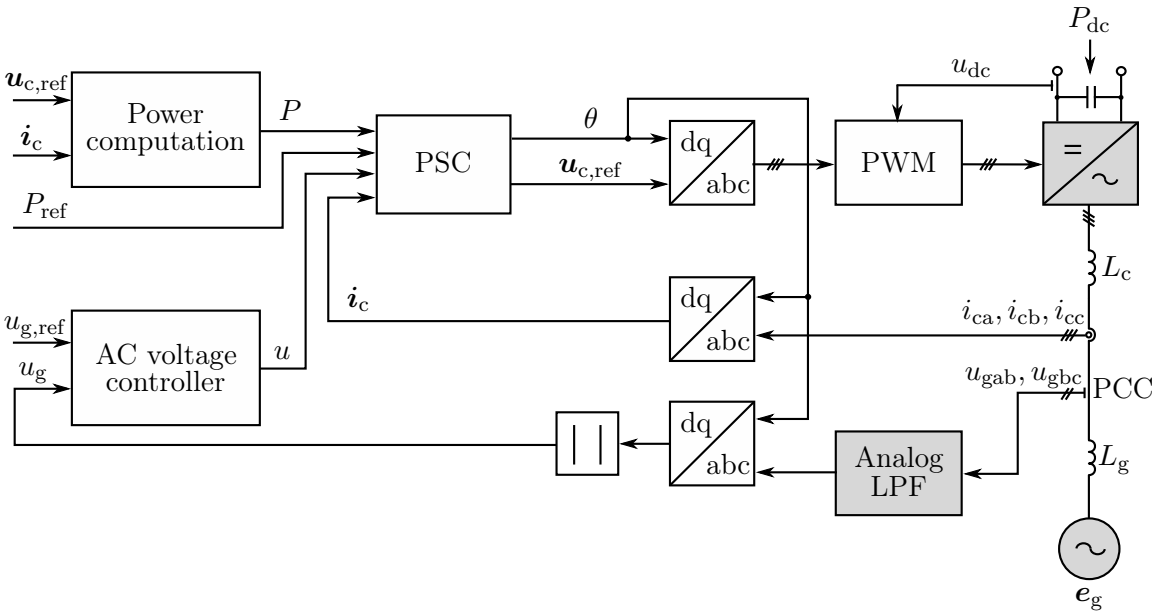

Figure 3.7: PSC with AC voltage controller.

Fig. 3.6 shows the block diagram of PSC control law, where ω_{PLL} is the signal coming from the PLL which is used to synchronize the converter to the grid for the first time. The PLL for PSC is discussed in more detail in Section 4.2.2. The over-all block diagram of PSC augmented with other necessary blocks is shown in Fig. 3.7

Fig. 3.8 shows the vector diagram of PSC-controlled converter drawn for two different operating points for weak grids. The AC-voltage controller is not used in this example case. The magnitude and angle of the vectors are determined from the steady state equations. The power-angle equation can be written as

$$P = \frac{u_c e_g \sin\delta}{\omega_g(L_c + L_g)} \tag{3.16}$$

For SCR = 1 and $u_c = e_g = 1$ p.u. , $P = \sin\delta$

where δ ranges from 0° to 90°. The maximum theoretical power that can flow for SCR = 1 is 1 p.u at $\delta = 90$. The vector diagram is plotted for two cases, i.e., $P =$ 0.5 p.u. and $P = 1$ p.u. The angle δ is 30° and 90° respectively. From the circuit in Fig. 3.1

$$\boldsymbol{i}_c = \frac{-j \cdot u_c + j \cdot e_g \angle -\delta}{\omega_g(L_c + L_g)} \quad ; \quad \boldsymbol{u}_g = u_c - j\omega_g L_c \boldsymbol{i}_c \tag{3.17}$$

From the vector diagrams (cf. Fig. 3.8), it can be interpreted that the amount of power flow in PSC-controlled converter is independent of the PCC voltage magnitude. Although, the PCC voltage magnitude drops with the increase in power flow.

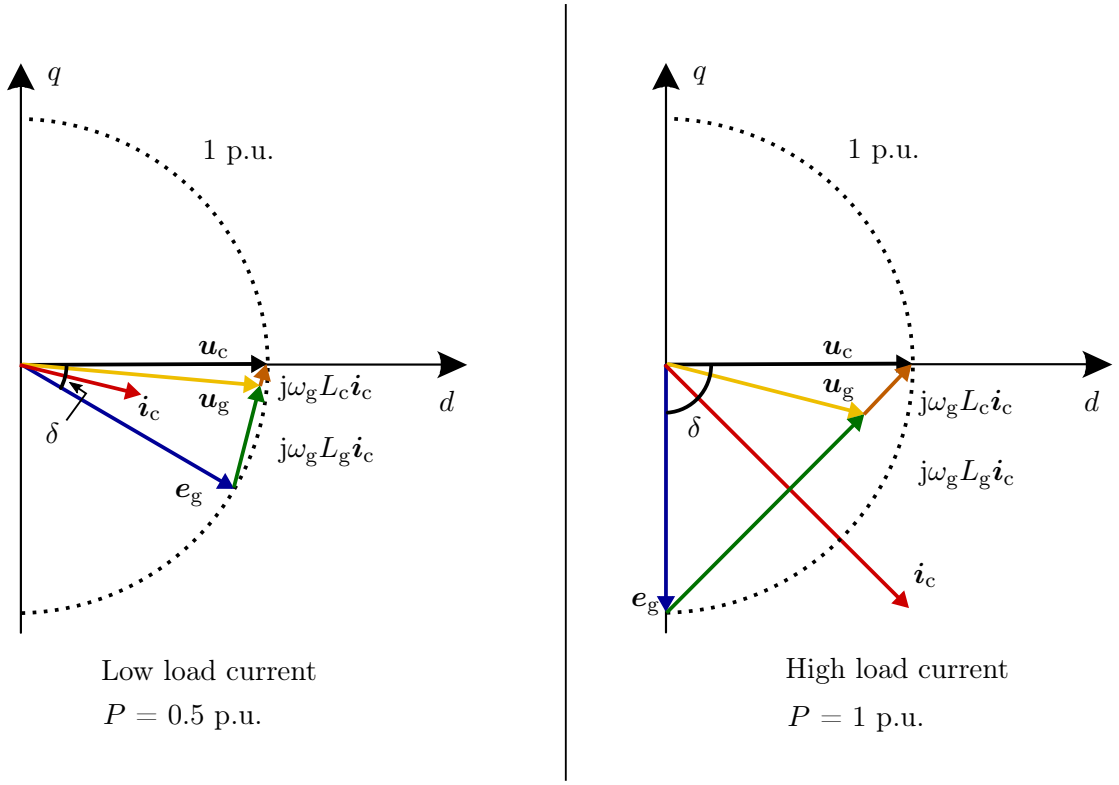

Figure 3.8: Vector diagram.

3.4 Vector Control with an Outer-loop Power Controller

Various control methods have already been introduced in the literature in order to improve the performance of the vector control scheme under weak-grid conditions [24,27,28]. Re-tuning of the PLL and outer-loop controllers are the typical solutions. It is a well known fact that an AC-voltage controller and a low PLL bandwidth is needed in weak-grid conditions in order to transfer 1 p.u. of the power [24]. There is strong coupling between the active and the reactive power in weak-grid conditions due to the PCC voltage dependency on the converter current. Also, the AC-voltage controller interfere with the performance of the PLL through the PCC voltage. Reduced PLL bandwidth allows the PLL output to be less sensitive to the changes in the PCC voltage. Otherwise, a fast PLL response affects the performance and quality of the transferred power and the system becomes poorly damped.

Another possible solution is to use an outer-loop active-power controller. The complete block diagram is shown in Fig. 3.9. An integral controller is used as the power controller. Here P is the measured power at the PCC. The AC-voltage controller interfere with the active-power regulation. Intuitively, the power controller should have smaller bandwidth as compared to the AC-voltage controller. As a result, it is easy for the PLL to track the PCC voltage angle without any need of reducing the PLL bandwidth. It is important to note that the same effect cannot be achieved by reducing the bandwidth of both the channels of the current controller. The

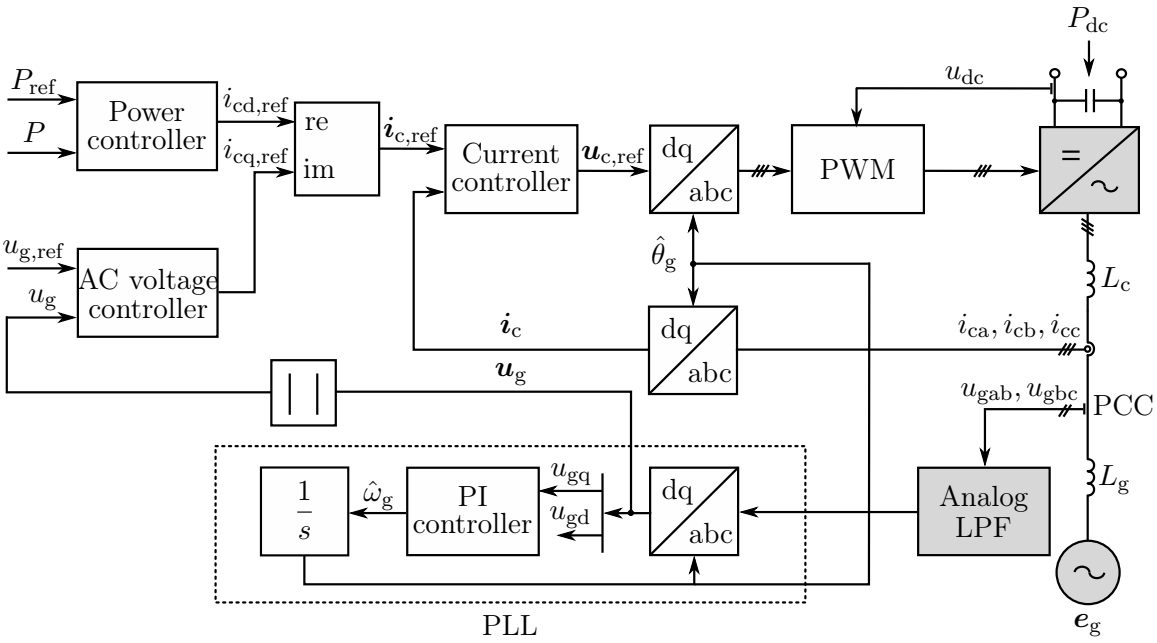

Figure 3.9: Vector control with an Outer-loop power controller.

closed-loop AC-voltage dynamics should be faster than the power-loop dynamics. One disadvantage of using this scheme is that the dynamic response of the system becomes slow also for strong grids. To make the dynamic response fast for strong grids, the power controller should be re-tuned. Re-tuning is not a feasible solution as it requires information of the grid impedance.

This implementation is a little different from the standard vector control scheme in a way that the current reference is not generated based on (3.5). The real component of the current reference is provided by the power controller and the imaginary component of the current reference is provided by the AC-voltage controller. These two components are combined together to establish a current reference for the inner current controller.

3.5 Modified Vector Control for Weak Grids

Two novel modified vector control schemes are being proposed in this section. The schemes are robust to the changes in the grid impedance. The schemes are discussed as follows

3.5.1 Scheme 1

In this scheme, the power reference (or the reference for the active-power-producing current component) is modified by feeding back the filtered converter-voltage reference or the measured converter voltage. One way to implement the modification

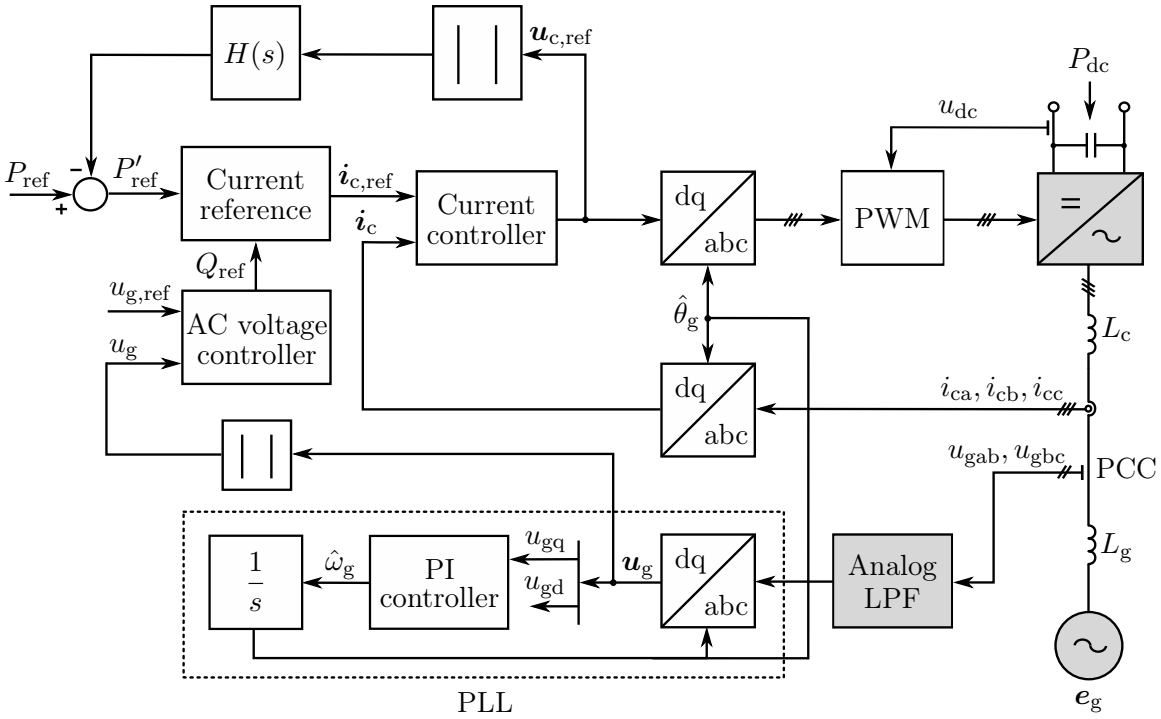

Figure 3.10: Example implementation of scheme 1.

is to subtract the high-pass filtered converter reference-voltage magnitude from the power reference. Also, the PLL bandwidth is needed to be reduced. Fig. 3.10 shows an example implementation of scheme 1, where the high-pass filtered converter reference-voltage magnitude is subtracted from the power reference. The modified power reference P'_{ref} is

$$P'_{\mathrm{ref}} = P_{\mathrm{ref}} - H(s)|\boldsymbol{u}_{\mathrm{c,ref}}| \tag{3.18}$$

where the high-pass filter $H(s)$ is

$$H(s) = \frac{K_{\mathrm{h}} s}{s + \alpha_{\mathrm{h}}} \tag{3.19}$$

The gain of the filter is K_{h} and the bandwidth is α_{h}. The high-pass filter damps the oscillations in the power flow.

The modification can also be implemented in an alternative way. Modify the power-producing current reference $i_{\mathrm{cd,ref}}$ instead of the power reference P_{ref}. In this case, the implementation can be seen as a modified current controller.

The scheme does not require the estimation of the grid impedance. Furthermore, the tuning of the control parameters is independent of the grid strength.

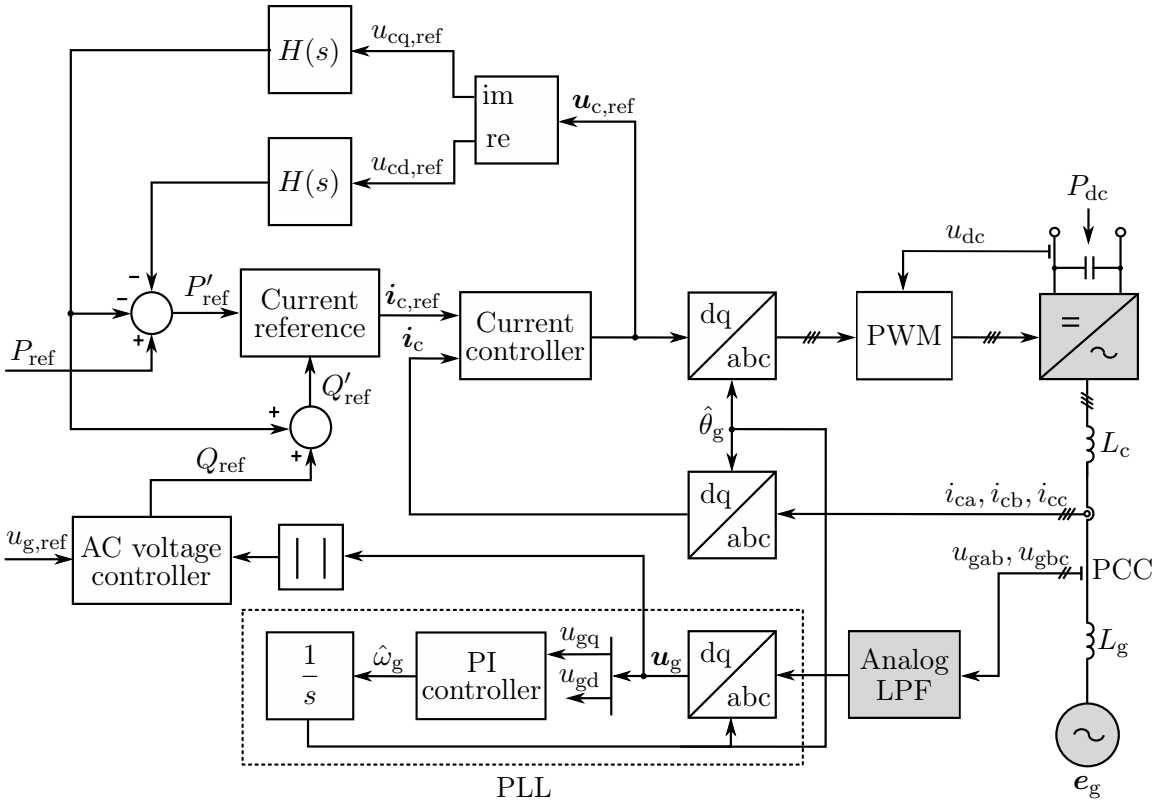

Figure 3.11: Example implementation of scheme 2.

3.5.2 Scheme 2

In this scheme, the active-power reference (or the reference for the active-power-producing current component) and the reactive-power reference (or the reference for the reactive-power-producing current component) are modified. The modification is implemented to damp the cross-coupling terms between the active and reactive power. The cross coupling appears in weak grids due to the inaccurate grid-voltage angle estimation by the PLL during transients or a fast PLL response to PCC voltage disturbances. The cross-coupling terms can be found from the small signal analysis

$$P = \frac{3}{2}\,\mathrm{Re}\,\{\boldsymbol{u}_{\mathrm{g}}\boldsymbol{i}_{\mathrm{c}}^{*}\} = \frac{3}{2}(u_{\mathrm{gd}}i_{\mathrm{cd}} + u_{\mathrm{gq}}i_{\mathrm{cq}}) \tag{3.20}$$

$$Q = \frac{3}{2}\,\mathrm{Im}\,\{\boldsymbol{u}_{\mathrm{g}}\boldsymbol{i}_{\mathrm{c}}^{*}\} = \frac{3}{2}(u_{\mathrm{gq}}i_{\mathrm{cd}} - u_{\mathrm{gd}}i_{\mathrm{cq}}) \tag{3.21}$$

The linearized equation with perturbed variables can be written as

$$\Delta P = \frac{3}{2}(u_{\mathrm{gd0}}\Delta i_{\mathrm{cd}} + \Delta u_{\mathrm{gd}}i_{\mathrm{cd0}} + \Delta u_{\mathrm{gq}}i_{\mathrm{cq0}}) \tag{3.22}$$

$$\Delta Q = \frac{3}{2}(-u_{\mathrm{gd0}}\Delta i_{\mathrm{cq}} - \Delta u_{\mathrm{gd}} i_{\mathrm{cq0}} + \Delta u_{\mathrm{gq}} i_{\mathrm{cd0}}) \tag{3.23}$$

The last two terms in the linearized equations are appearing due to the error in the grid-voltage phase estimation.

High-pass filtered grid voltage components should be subtracted from the active and reactive power references based on the above analysis. It is found that using the converter-voltage reference (or the measured converter voltage) instead of the measured grid voltage is more effective in damping the oscillations in power. Fig. 3.11 shows an example implementation of scheme 2. The active and reactive power references can be chosen as

$$P_{\mathrm{ref}}^{'} = P_{\mathrm{ref}} - H(s)u_{\mathrm{cd,ref}} - H(s)u_{\mathrm{cq,ref}} \tag{3.24}$$

$$Q_{\mathrm{ref}}^{'} = Q_{\mathrm{ref}} - H(s)u_{\mathrm{cq,ref}} \tag{3.25}$$

where the high-pass filter $H(s)$ is

$$H(s) = \frac{K_{\mathrm{h}} s}{s + \alpha_{\mathrm{h}}} \tag{3.26}$$

The filtered real component of the converter-voltage reference is not subtracted from the reactive-power reference. The reason is that the response of the system does not change. The modification can also be implemented in an alternative way. The filtered converter-voltage reference components can be directly subtracted from the reference real and imaginary current components. So this modification can be implemented in the current controller.

4 Parameters Selection of the Controllers

In this section, the parameters selection of the controllers is discussed. The choice of controllers is based on the requirement that the control schemes resemble as closely as possible. In this way, the comparison of these schemes becomes easier and reliable. The common controllers are discussed only once.

4.1 Vector Current Controller

Current controller is an important part of the vector control scheme. A basic PI controller is commonly used as a current controller. The current controller should have a fast transient response and good enough damping characteristics. The differential equation in synchronous coordinates can be written as

$$L_\mathrm{c}\frac{d\boldsymbol{i}_\mathrm{c}}{dt} + \mathrm{j}\omega_\mathrm{g}L_\mathrm{c}\boldsymbol{i}_\mathrm{c} = \boldsymbol{u}_\mathrm{c} - \boldsymbol{u}_\mathrm{g} \tag{4.1}$$

The transfer function of the plant to be controlled can be written as

$$\frac{\boldsymbol{i}_\mathrm{c}(s)}{\boldsymbol{u}_\mathrm{c}(s)} = Y_\mathrm{g}(s) = \frac{1}{(s+\mathrm{j}\omega_\mathrm{g})L_\mathrm{c}} \tag{4.2}$$

The PCC voltage $\boldsymbol{u}_\mathrm{g}$ can be seen as a load disturbance. The term $\mathrm{j}\omega_\mathrm{g}L_\mathrm{c}\boldsymbol{i}_\mathrm{c}$ causes cross coupling between the d and q axis.

$$L_\mathrm{c}\frac{di_\mathrm{cd}}{dt} = u_\mathrm{cd} - u_\mathrm{gd} + \omega_\mathrm{g}L_\mathrm{c}i_\mathrm{cq} \tag{4.3}$$

$$L_\mathrm{c}\frac{di_\mathrm{cq}}{dt} = u_\mathrm{cq} - u_\mathrm{gq} - \omega_\mathrm{g}L_\mathrm{c}i_\mathrm{cd} \tag{4.4}$$

In order to remove the effect of cross-coupling in the closed-loop system, the term $\mathrm{j}\omega_\mathrm{g}L_\mathrm{c}\boldsymbol{i}_\mathrm{c}$ is added to the controller output. The active damping resistance r is also

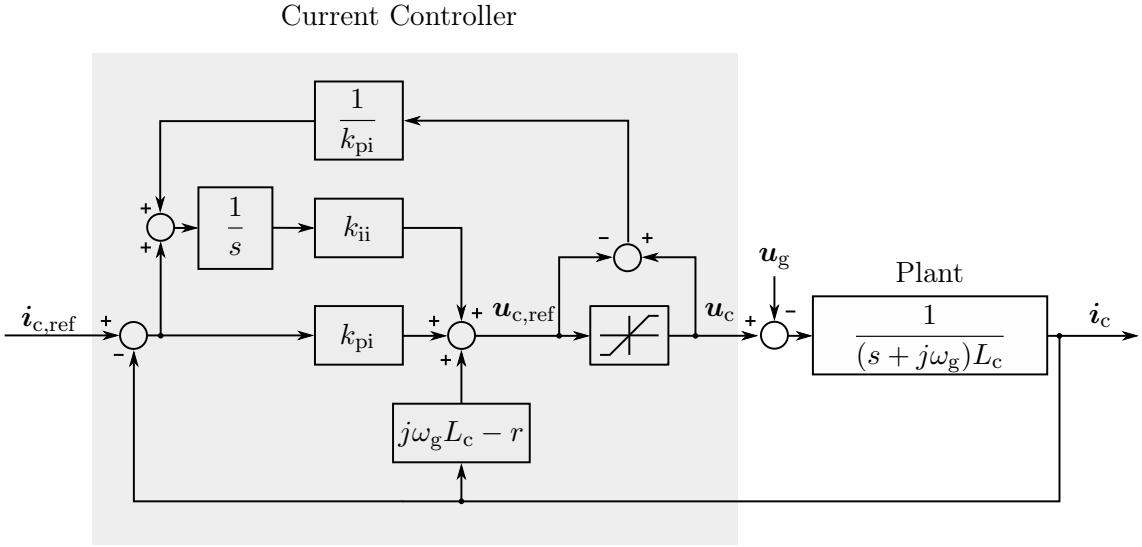

Figure 4.1: Back-calculation anti-windup.

included in the controller to improve the disturbance rejection capability. The resulting plant model as seen from the PI controller can be written as

$$Y'_{\mathrm{g}}(s) = \frac{1}{sL_{\mathrm{c}} + r} \tag{4.5}$$

The bandwidth of $Y'_{\mathrm{g}}(s)$ can be selected to be α_{c}. This gives the selection of r to be

$$r = \alpha_{\mathrm{c}} L_{\mathrm{c}} \tag{4.6}$$

In order to find the proportional and integral gains k_{pi} and k_{ii} respectively, the internal model control principle can be used [29]. Equating the closed-loop transfer function with the desired one gives

$$G(s) = \frac{K(s)Y'_{\mathrm{g}}(s)}{1 + K(s)Y'_{\mathrm{g}}(s)} = \frac{\alpha_{\mathrm{c}}}{s + \alpha_{\mathrm{c}}} \tag{4.7}$$

where $K(s)$ is the transfer function of the PI controller and α_{c} is the desired bandwidth of the closed-loop system.

$$k_{\mathrm{pi}} = \alpha_{\mathrm{c}} L_{\mathrm{c}} \qquad\qquad k_{\mathrm{ii}} = \alpha_{\mathrm{c}} r = \alpha_{\mathrm{c}}^2 L_{\mathrm{c}} \tag{4.8}$$

The bandwidth α_{c} should be at least one decade smaller than the sampling frequency.

The maximum converter output voltage $\boldsymbol{u}_{\mathrm{c}}$ is limited. The maximum limit is decided by the DC-link voltage u_{dc}. The reference voltage $\boldsymbol{u}_{\mathrm{c,ref}}$ may exceed the maximum realizable voltage. This can result in the overflow of the integration memory. An

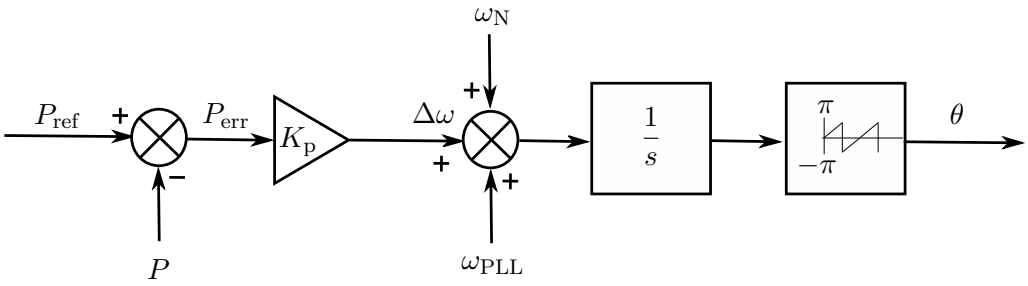

Figure 4.2: Active-power controller.

anti-windup scheme is used to avoid the overflow of the memory. The controller block diagram with an anti-windup is shown in Fig. 4.1

4.2 PSC

The tuning and parameter selection of the controllers used in PSC are discussed here.

4.2.1 Active-Power Controller

The active-power controller (APC) shown in Fig. 4.2 is used in PSC to serve two purposes. 1) It is used to regulate the active power transferred from the converter to the grid or vice-versa ; 2) it keeps the converter synchronized with the grid. The output of an APC is the change in the phase angle between the converter and the grid voltage. The input is the error between the reference power and the measured power. A simple integral controller is used to regulate the power. The gain of the controller K_p is selected as:

$$K_p = \frac{2\omega_N R}{3u^2} \tag{4.9}$$

The above selection criteria comes from the gain margin of the open loop transfer function from P_{ref} to P [25]. The above selection criteria depends upon the converter voltage magnitude. This kind of technique is used for the control of non-linear systems using linear controllers. This technique is called gain scheduling.

The nominal angular frequency ω_N is added to the angular frequency increment $\Delta\omega$. The output from the PLL is also added to the input of the integrator. The output of APC is kept between π and -π to avoid numerical overflow of the integrator.

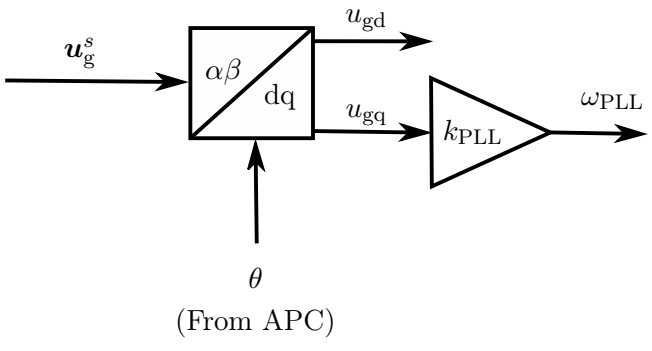

Figure 4.3: Phase-locked loop for PSC.

4.2.2 Phase-Locked Loop

Fig. 4.3 shows the PLL used by PSC to synchronize the converter to the grid before the converter starts its operation. Once the converter is synchronized with the grid, the PLL is no longer needed. PLL is usually very fast at tracking the grid voltage angle and there is almost no need to wait for the system to be synchronized. The PLL is removed from the system before PSC starts its operation. Synchronization is maintained by PSC through APC. The gain k_{PLL} is selected by trial and error. The PLL used by PSC works on the same principle as the one discussed for vector control.

4.3 Common Controllers

4.3.1 DC-link Controller

An outer-loop DC-link controller is often used with a VSC to maintain the DC-link voltage to a set value. DC-link voltage control can be classified as a regulation problem. A DC-link consists of a capacitor. The dynamics of the DC-link can be expressed in terms of the amount of energy W_{d} stored in the DC-link capacitor as

$$sW_{\mathrm{dc}} = P_{\mathrm{dc}} - P \tag{4.10}$$

where P_{dc} is the DC-source power which acts like a disturbance in DC-link control and P is the output power of the converter. The converter is assumed to be lossless. The DC-link energy is related to the DC-link voltage and DC-link capacitor as

$$W_{\mathrm{dc}} = \frac{1}{2} C_{\mathrm{dc}} u_{\mathrm{dc}}^2 \tag{4.11}$$

The block diagram of the DC-link control is shown in Fig. 4.4. The DC-link control law can be defined as

$$P_{\mathrm{ref}} = k_{\mathrm{dc}}(W_{\mathrm{dc}} - W_{\mathrm{dc,ref}}) + P_{\mathrm{dc,ff}} \tag{4.12}$$

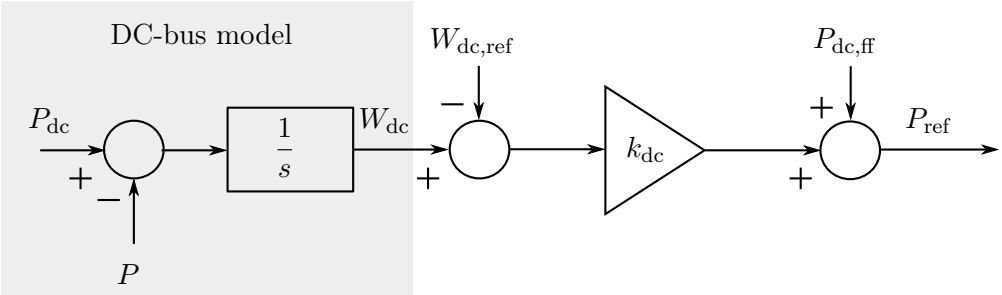

Figure 4.4: DC-link control.

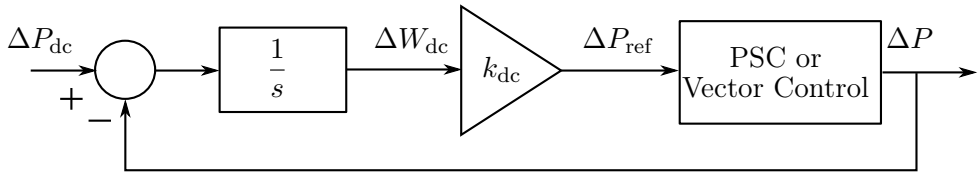

Figure 4.5: Closed-loop system.

where k_{dc} is the proportional gain of the DC-link controller, $P_{\mathrm{dc,ff}}$ is the low-pass filtered DC-source power P_{dc} used as a feed-forward. The reference DC-link energy can be calculated from the reference DC-link voltage as

$$W_{\mathrm{dc,ref}} = \frac{1}{2} C_{\mathrm{dc}} u_{\mathrm{dc,ref}}^2 \tag{4.13}$$

A total closed-loop system with perturbation quantities is shown in Fig. 4.5. PSC or vector control can be assumed to be faster than the DC-link control loop, i.e., $\Delta P_{\mathrm{ref}} = \Delta P$ can be assumed. The closed-loop transfer function becomes

$$G_{\mathrm{dc}}(s) = \frac{k_{\mathrm{dc}}}{s + k_{\mathrm{dc}}} \tag{4.14}$$

where k_{dc} is the bandwidth of the closed-loop DC-link control. The response of the closed-loop DC-link control is desired to be in the range of tens of milliseconds. This gives the closed-loop bandwidth k_{dc} of 0.1 to 0.2 p.u. The assumption $\Delta P_{\mathrm{ref}} = \Delta P$ does not hold in the case of vector control with an outer-loop power controller (cf. Fig. 3.9) due to the small bandwidth of the active-power controller. In this case, the gain k_{dc} should be reduced.

4.3.2 AC-Voltage Controller

As already discussed in Section 3.1, an AC-voltage controller is needed in weak grids to maintain the PCC voltage at 1 p.u. A PI controller is used as an AC-voltage controller. The output of the AC-voltage controller is used to feed different signals in different schemes. In PSC, the output of the AC-voltage controller is used

as the converter voltage magnitude u. In vector control, the output of the AC-voltage controller can be used as a reactive power reference Q_{ref} or a reactive power producing current component reference $i_{\mathrm{cq,ref}}$. The parameters of the controller are chosen using trial and error method.

5 Simulation Results

The simulation results of the control schemes discussed in Section 3 are presented in this section. The control schemes are tested for both strong grid (SCR = 5) and weak grid (SCR = 1) conditions. The parameters of the system are given in Table 5.1.

Table 5.1: System Parameters

Parameter	Actual value	Normalized value
Rated apparent power S_{ac}	12.5 kVA	1 p.u.
Rated voltage	$\sqrt{2/3}\cdot$ 400 V	1 p.u.
Rated current	$\sqrt{2}\cdot$ 18.3 A	1 p.u.
Base impedance	12.6 Ω	1 p.u.
Filter inductance L_{c}	8 mH	0.2 p.u.
DC-link voltage u_{dc}	650V	2 p.u.
DC-link capacitor C_{dc}	2.1 mF	8.3 p.u.
Nominal frequency f_{N}	50 Hz	1 p.u.
Switching frequency f_{sw}	4kHz	80 p.u.

Time domain simulations are used to compare the performance of all the control schemes discussed previously. Two modes of operation are tested in the simulations, i.e., active-power control mode and DC-link voltage control mode. Active-power steps P_{ref} steps are provided manually in the active-power control mode, assuming the DC-link voltage to be constant. DC-link voltage control mode is tested against the step changes in DC-source power P_{dc}. The control parameters of each scheme are listed in their respective sections. Although the AC-voltage controller can be omitted from PSC, it is used in each scheme under weak-grid conditions in order to reach the same operating point and make the comparison fair. The AC-voltage controller is turned off for strong grids. The simulation results are presented in the dq synchronous frame whose d-axis is aligned to the PCC voltage $\boldsymbol{u}_{\text{g}}$.

5.1 Standard Vector Control

The state-of-the-art standard vector control scheme is tested for strong and weak-grid conditions using simulations. The simulation results correspond to the control structure shown in Fig. 3.3. The parameters of the scheme are listed in Table 5.2. Fig. 5.1 shows the step response of standard vector control for strong grids. As discussed in Section 3.1, the response of standard vector control is very fast and it follows the reference power very well under strong-grid conditions. The dotted red line in the voltage plot shows the linear range of the modulator which is $u_{\mathrm{dc}}/\sqrt{3}$. It can be seen that the modulator saturates during the transients where the converter voltage magnitude u_{c} crosses $u_{\mathrm{dc}}/\sqrt{3}$ as discussed in Section 3.3

Table 5.2: Standard Vector Control Parameters

Parameter	Actual value	Normalized value
Current controller bandwidth α_{c}	1256 rad/s	4 p.u.
PLL Bandwidth	125 rad/s	1 p.u.
DC-link controller gain k_{dc}	56 rad/s	0.18
AC-voltage controller integral gain	6000 A/s	-
AC-voltage controller proportional gain	8 A	-

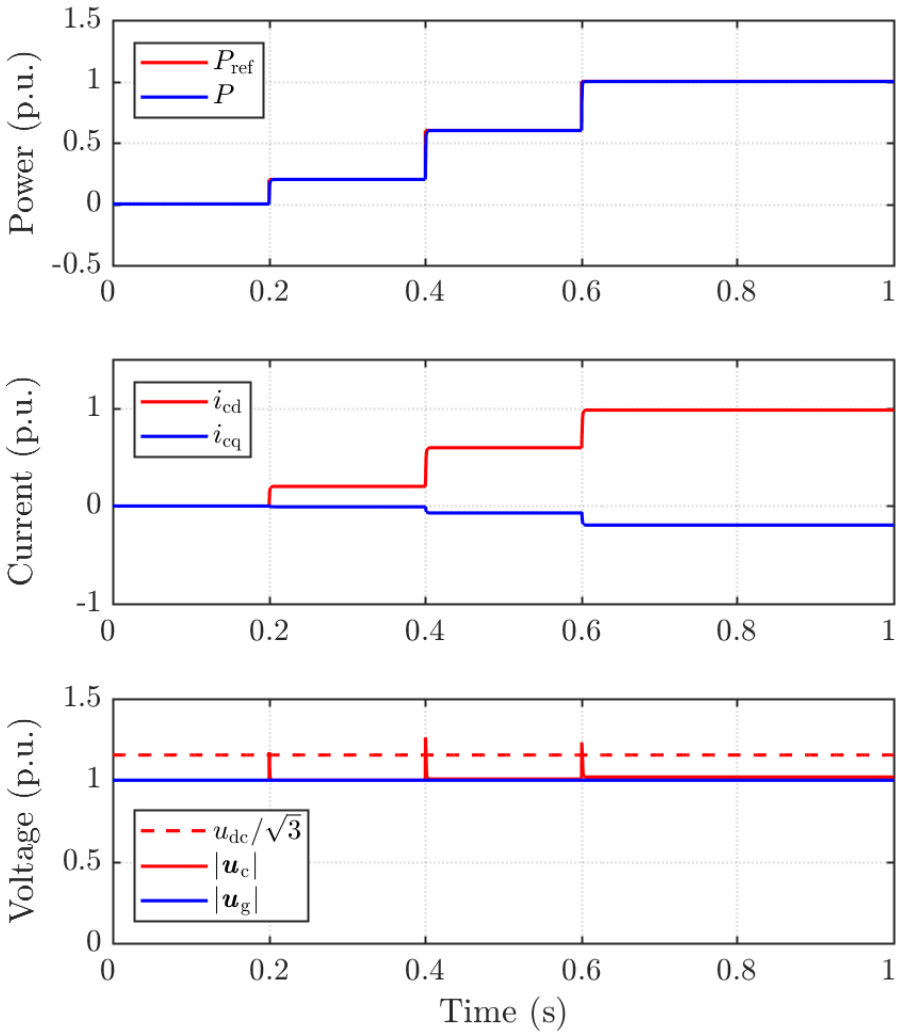

Figure 5.1: Step response of standard vector control for the strong grid.

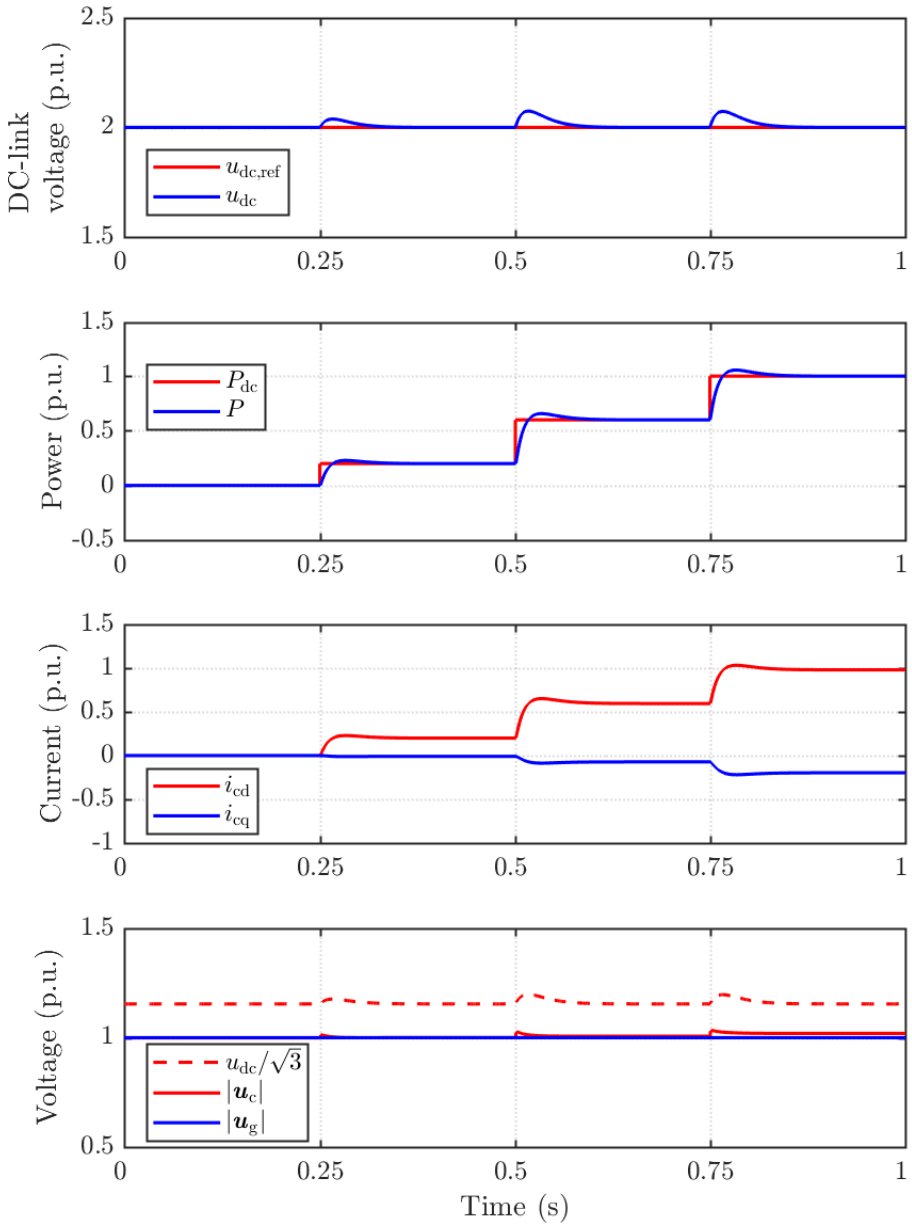

Figure 5.2: Step response of standard vector control with the cascaded DC-link control for the strong grid.

Fig. 5.2 shows the step response of standard vector control with the cascaded DC-link controller for the strong grid. The scheme seems to work very well at maintaining the DC-link voltage against the DC power flow variations, which acts as a disturbance.

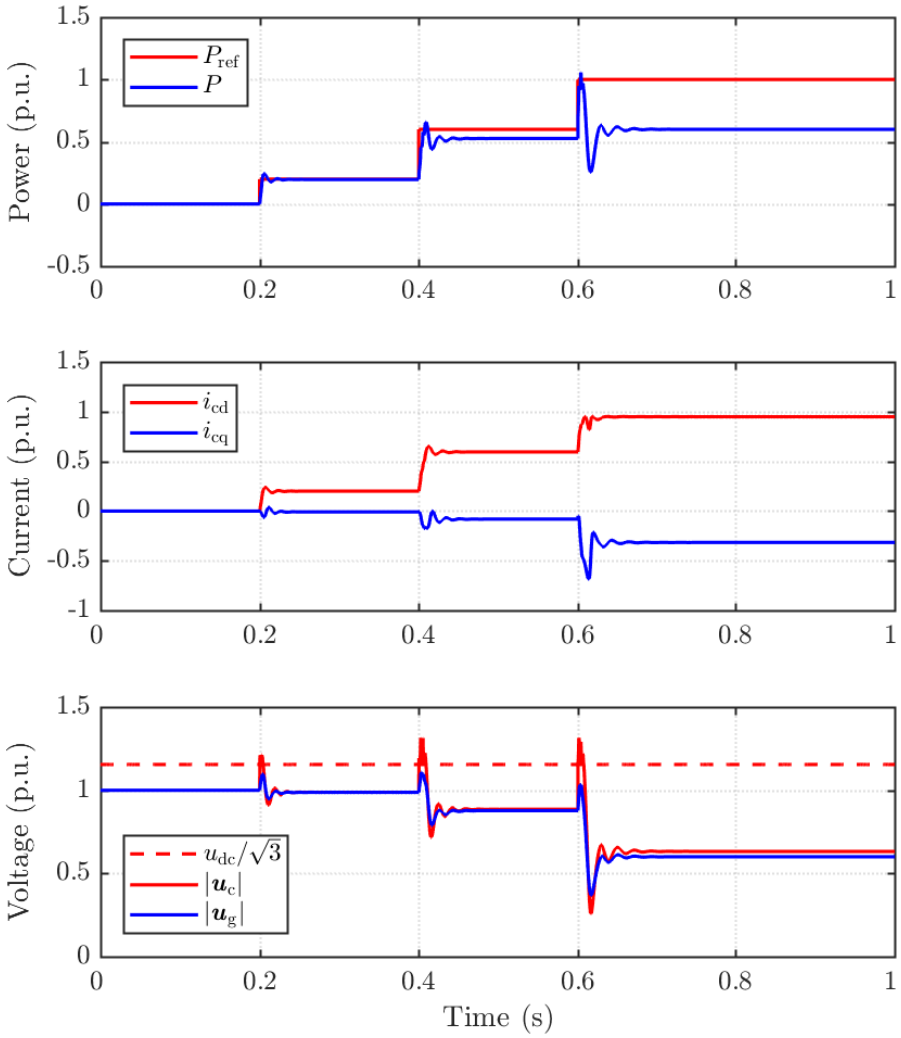

Figure 5.3: Step response of standard vector control for the weak grid.

Fig. 5.3 shows the response of standard vector control for the weak grid. The control scheme is unable to follow the power reference P_{ref}. The magnitude of the PCC voltage reduces with the increase in converter current. The power flow is limited to approximately 0.6 p.u. The results are corresponding to the analysis done in Section 3.1.2 based on vector diagrams.

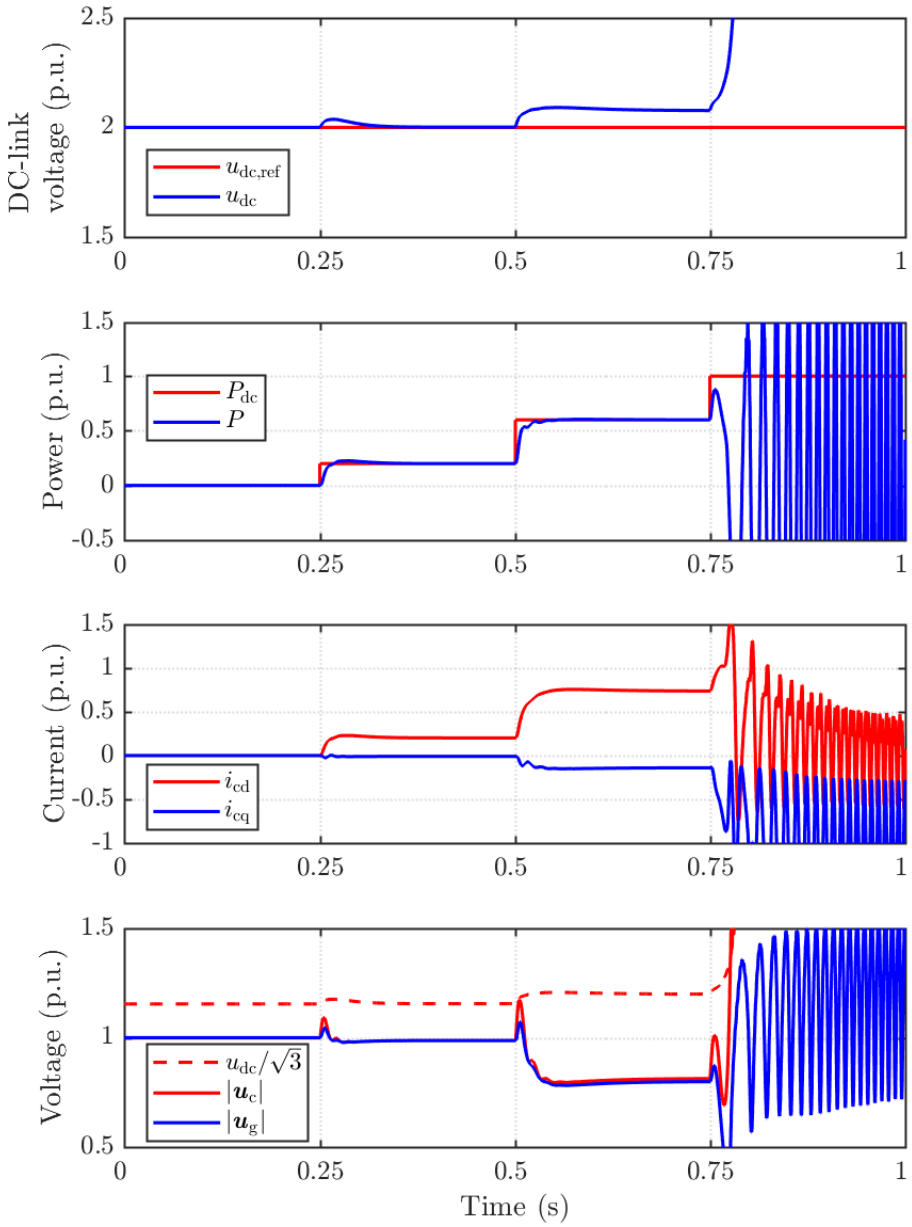

Figure 5.4: Step response of standard vector control with cascaded DC-link control for the weak grid.

When the DC-link controller is cascaded with the standard vector control scheme under weak-grid conditions, the resulting system becomes unstable as shown in Fig. 5.4. The DC-link controller is unable to maintain the DC-link voltage at 2 p.u. The reason is that the standard vector control scheme is unable to transfer more than 0.6 p.u. of the power. When the DC power P_{dc} is higher than the converter output power P, the surplus energy starts accumulating in the capacitor C_{dc}. As a result at 0.75 s instant, the DC-link voltage keeps increasing boundlessly.

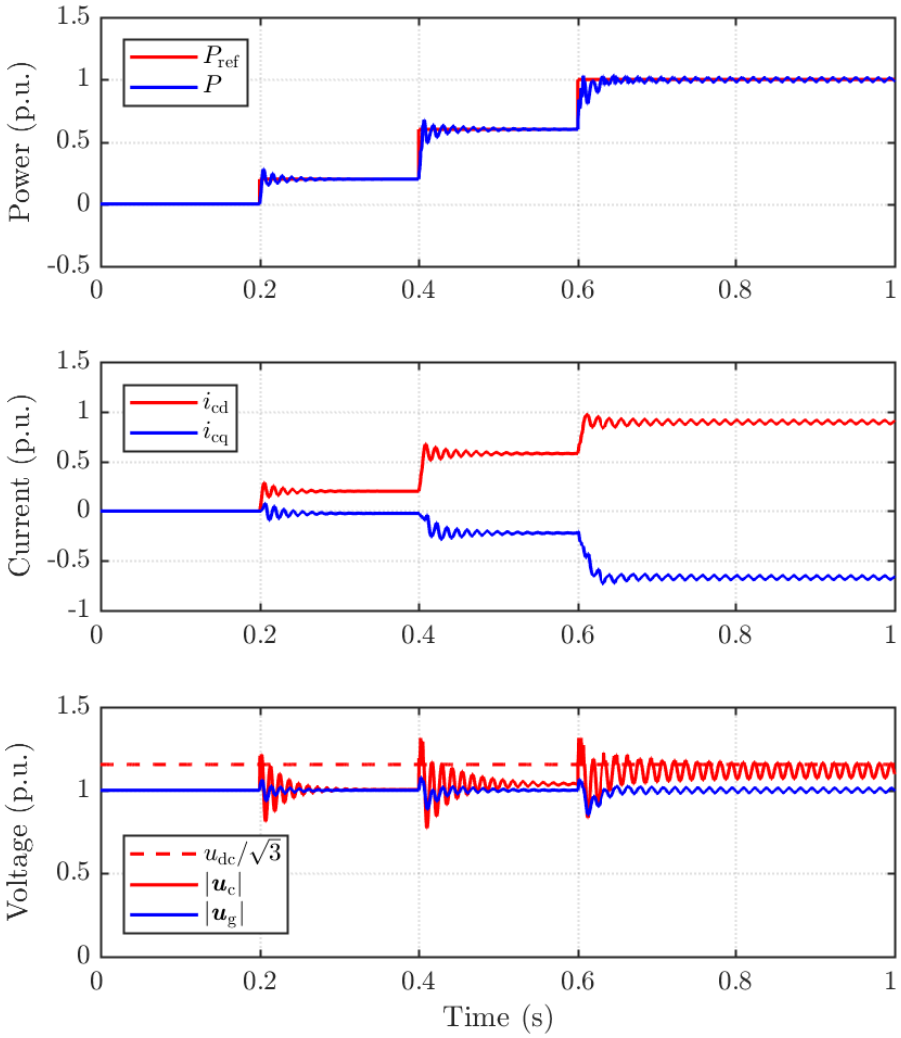

Figure 5.5: Step response of standard vector control with the cascaded AC-voltage controller for the weak grid, PLL bandwidth = $2\pi{\cdot}20$ rad/s.

In order to deal with the PCC voltage collapse in weak-grid conditions, the standard vector control can be augmented with an AC-voltage controller. The results are presented in Fig. 5.5. Although the scheme is able to transfer 1 p.u. of the power, the response becomes poorly damped due to the fast PLL response as discussed in Section 3.4.

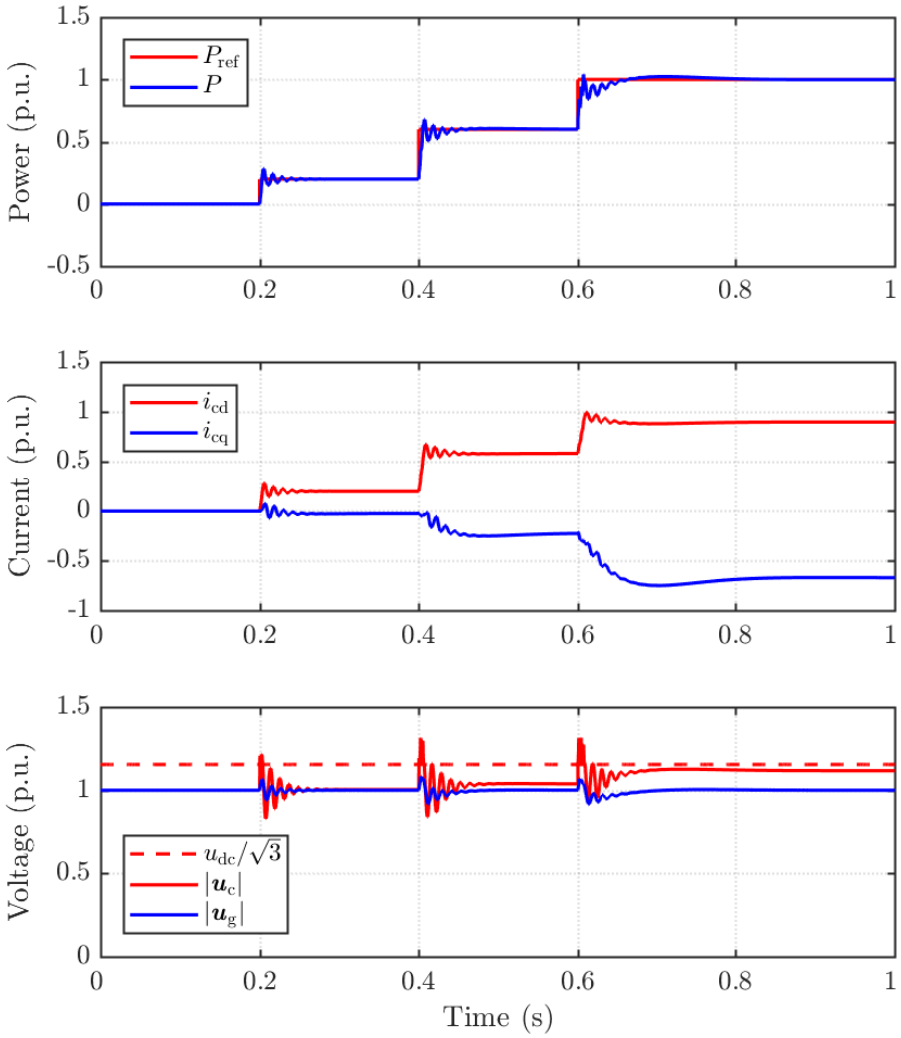

Figure 5.6: Step response of standard vector control with cascaded AC-voltage control for the weak grid, PLL bandwidth = $2\pi{\cdot}5$ rad/s.

If we reduce the PLL bandwidth, the oscillations can be reduced as shown in Fig. 5.6. On the downside, it takes more time now to reach the steady state due to the slow-tracking PLL and low frequency oscillations are present. This proves that the PLL has an affect on the performance of VSCs connected to weak grids.

5.2 Vector Control with an Outer-loop Power Controller

This section presents the simulation results of the vector control scheme with an outer-loop power controller (cf. Fig. 3.9). The parameters of the control scheme are listed in Table 5.3. Figs. 5.7 and 5.8 show the simulation results of the active-power control and DC-link voltage control, respectively. The controllers are tuned for the worst case scenario (weak grid). The response can be made faster for strong grids with the re-tuning of the controllers but it is not preferable to re-tune the controllers based on the changing SCR.

Table 5.3: Parameters of Vector Control with an Outer-loop Power Controller

Parameter	Actual value	Normalized value
Current controller bandwidth α_c	1256 rad/s	4 p.u.
PLL Bandwidth	125 rad/s	0.4 p.u.
DC-link controller gain k_{dc}	25 rad/s	0.08
AC-voltage controller integral gain	25 A/(V.s)	-
AC-voltage controller proportional gain	1 A/V	-
Power controller integral gain	0.15/V	-

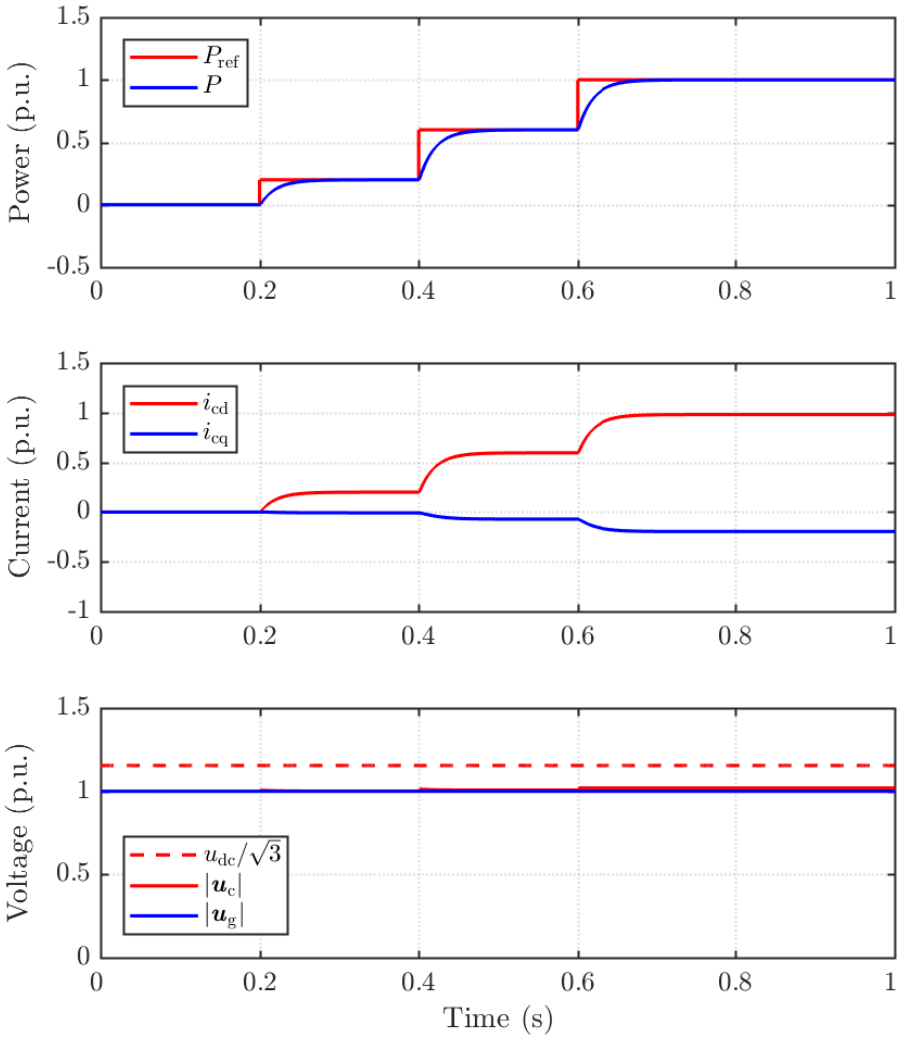

Figure 5.7: Step response of vector control with an outer-loop power controller for the strong grid.

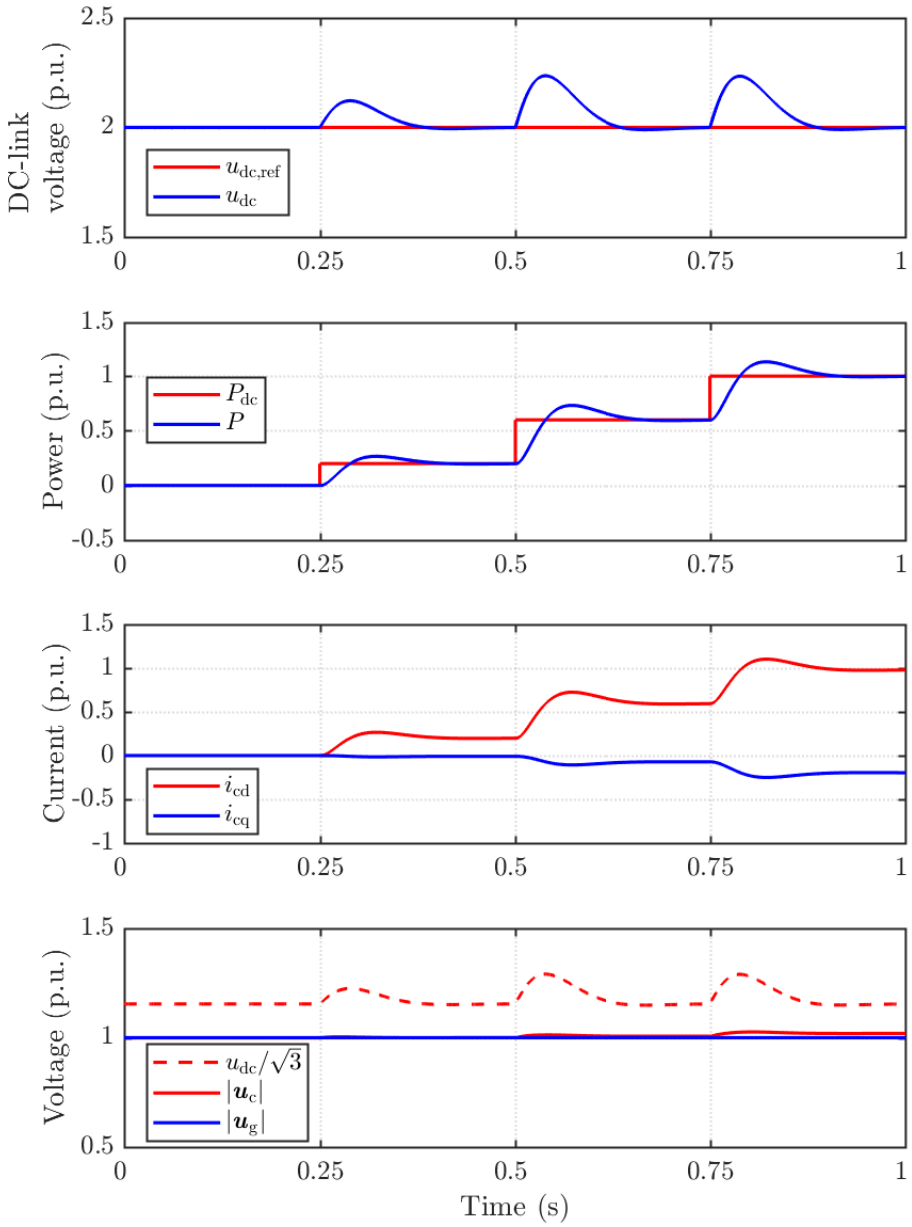

Figure 5.8: Step response of vector control with an outer-loop power controller and the cascaded DC-link controller for the strong grid.

The regulation of the DC-link voltage is slow due to the small bandwidth of the active-power controller. The deviation in the DC-link voltage from the reference value during the transients is bigger than in the standard vector control scheme (cf. Fig. 5.2).

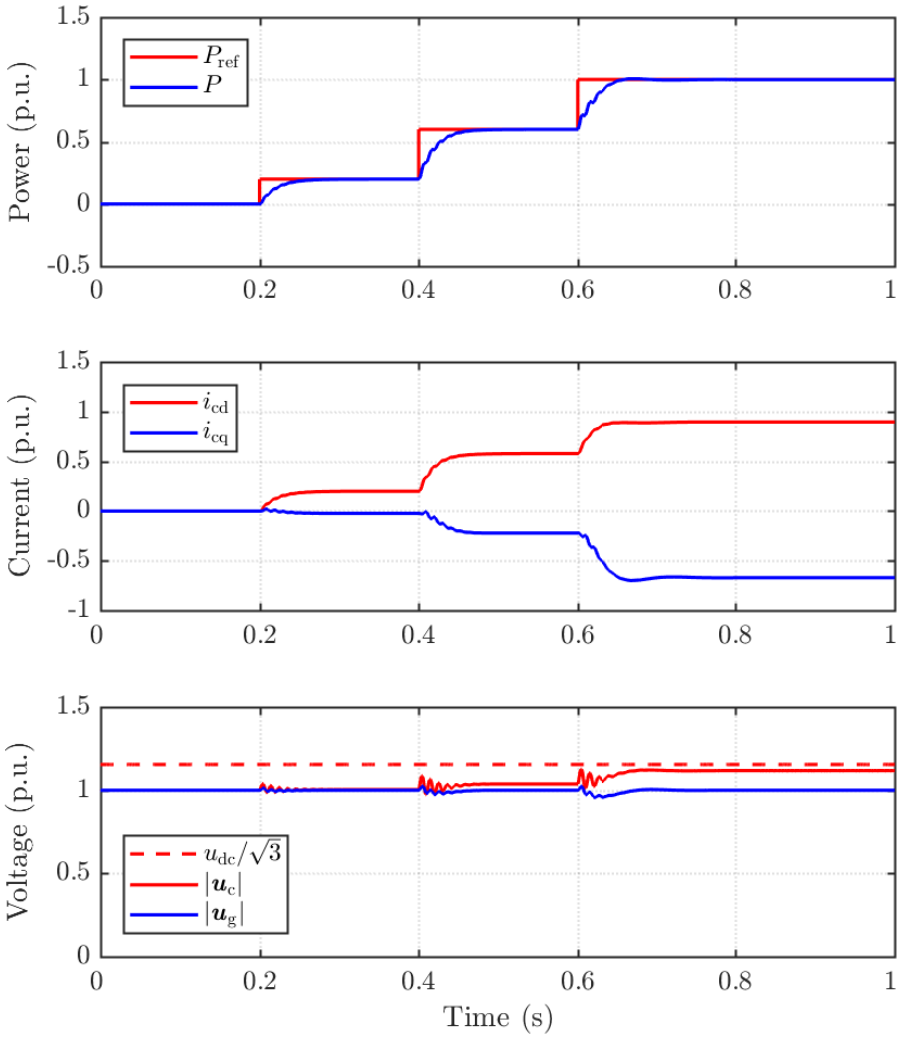

Figure 5.9: Step response of vector control with an outer-loop power controller for the weak grid.

The response for weak-grid conditions is shown in Fig. 5.9. The quality of the power has improved greatly. The oscillations in the power are very less as compared to the response of the standard vector control (cf. Fig. 5.6).

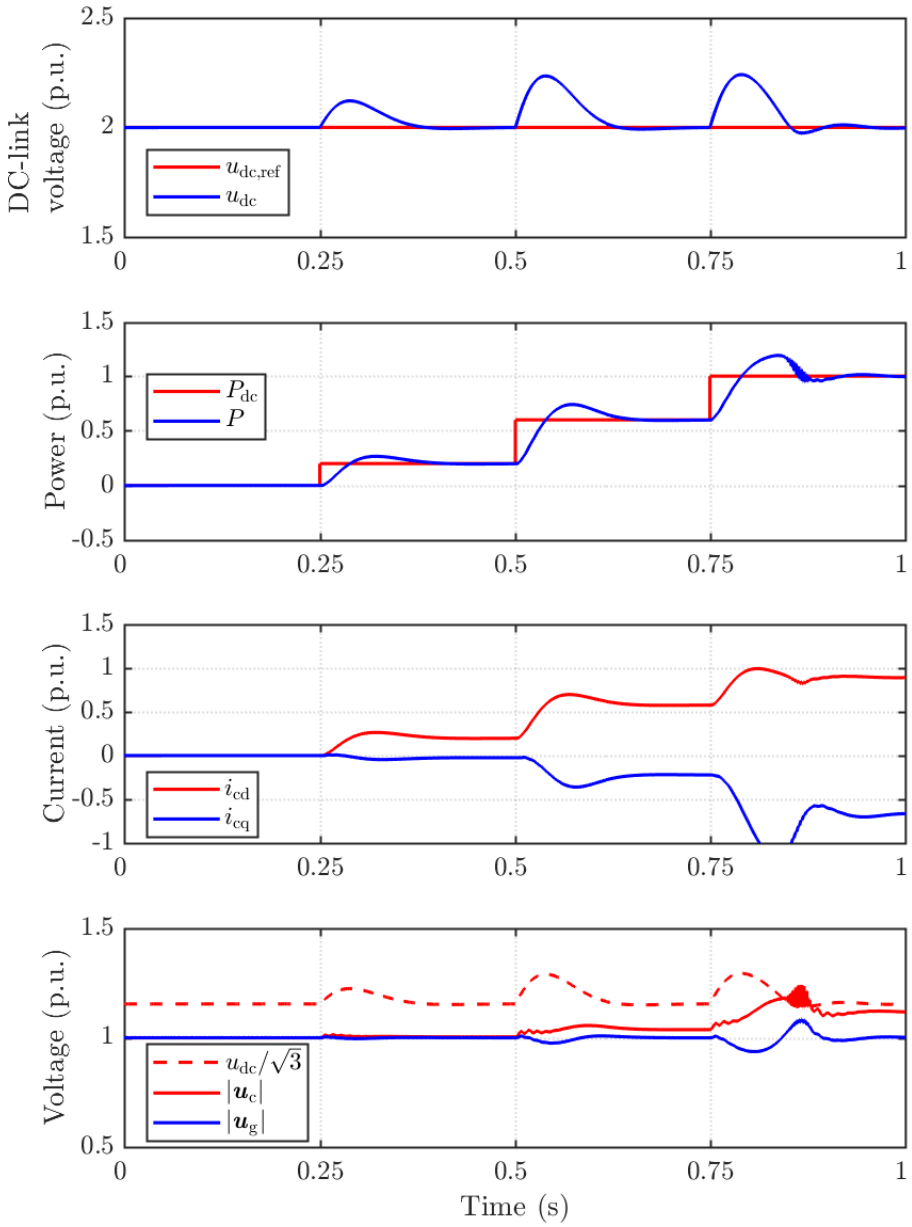

Figure 5.10: Step response of vector control with an outer-loop power controller and the cascaded DC-link control for the weak grid.

Fig. 5.10 shows the simulation results of the scheme with the cascaded DC-link controller for the weak grid. Although the system is stable and the DC-link controller is able to regulate the DC-link voltage, the response is very slow. Besides this, the AC voltage profile is also distorted and the modulator is going into the saturation region.

5.3 Modified Vector Control: Scheme 1

The modified vector control scheme discussed in Section 3.5.1 is also tested with the simulations. Table 5.4 presents the parameters of the control scheme. The working of the modified vector control is tested for strong-grid conditions and the results are presented in Figs. 5.11 and 5.12. The modified vector control works almost as good as the standard vector control scheme for strong-grid conditions (cf. Figs. 5.1 and 5.2).

Table 5.4: Modified Vector Control Parameters

Parameter	Actual value	Normalized value
Current controller bandwidth α_c	1256 rad/s	4 p.u.
PLL Bandwidth	31 rad/s	0.1 p.u.
High-pass filter bandwidth α_h	31 rad/s	0.1 p.u.
High-pass filter gain K_h	25.88	-
AC-voltage controller integral gain	6000 A/s	-
AC-voltage controller proportional gain	80 A	-

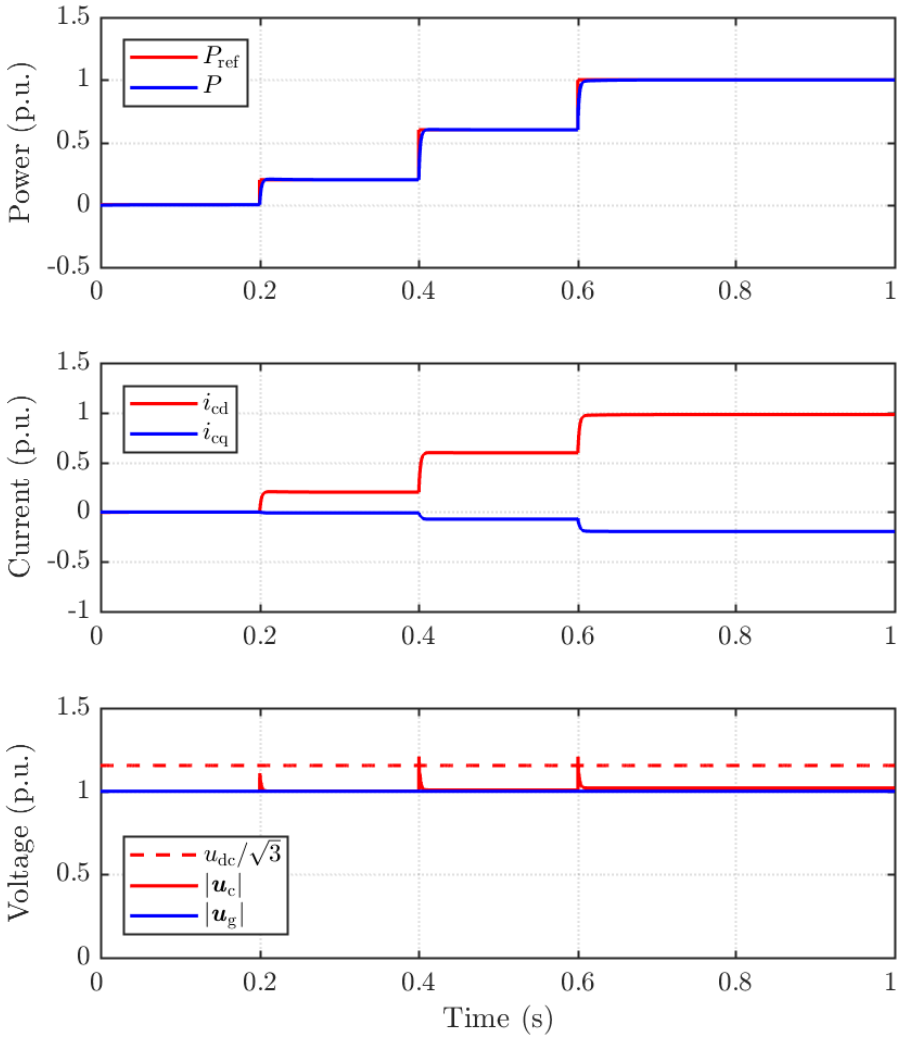

Figure 5.11: Step response of the modified vector control scheme 1 for the strong grid.

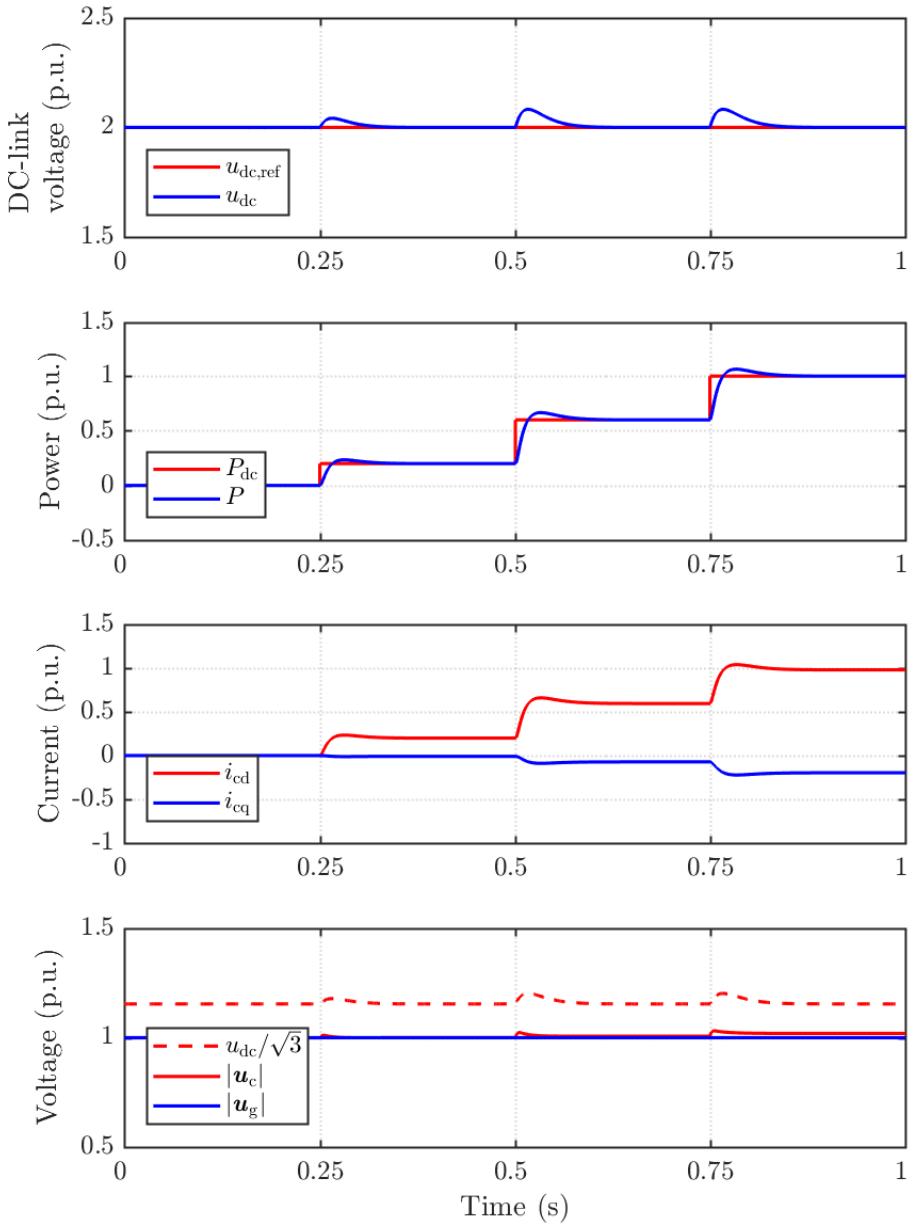

Figure 5.12: Step response of the modified vector control scheme 1 with the cascaded DC-link control for the strong grid.

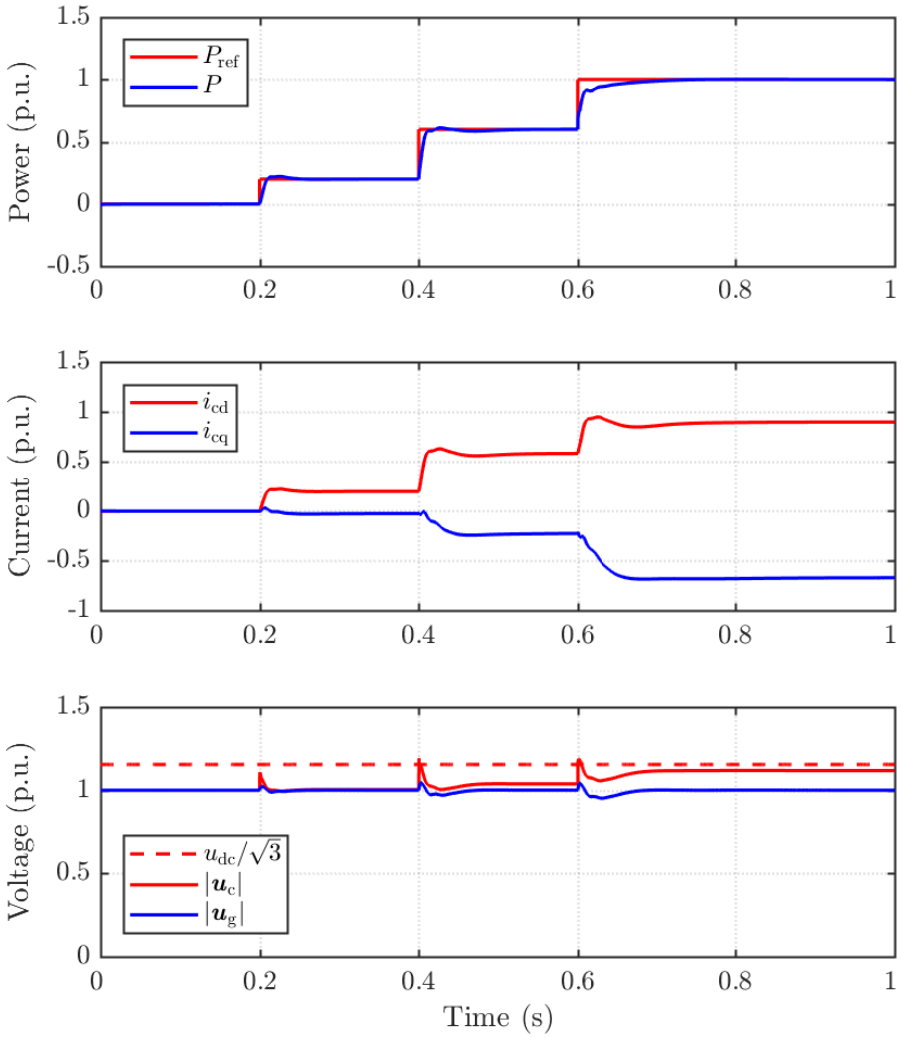

Figure 5.13: Step response of the modified vector control scheme 1 for the weak grid.

The step response for the weak grid is shown in Fig. 5.13. The response is clearly better than the one shown in Fig. 5.6. The scheme provides sufficient damping and the oscillations from the power are eliminated. The AC-voltage controller is fast enough to restore the PCC voltage without large oscillations. The modulator is saturating during transients for a very short duration.

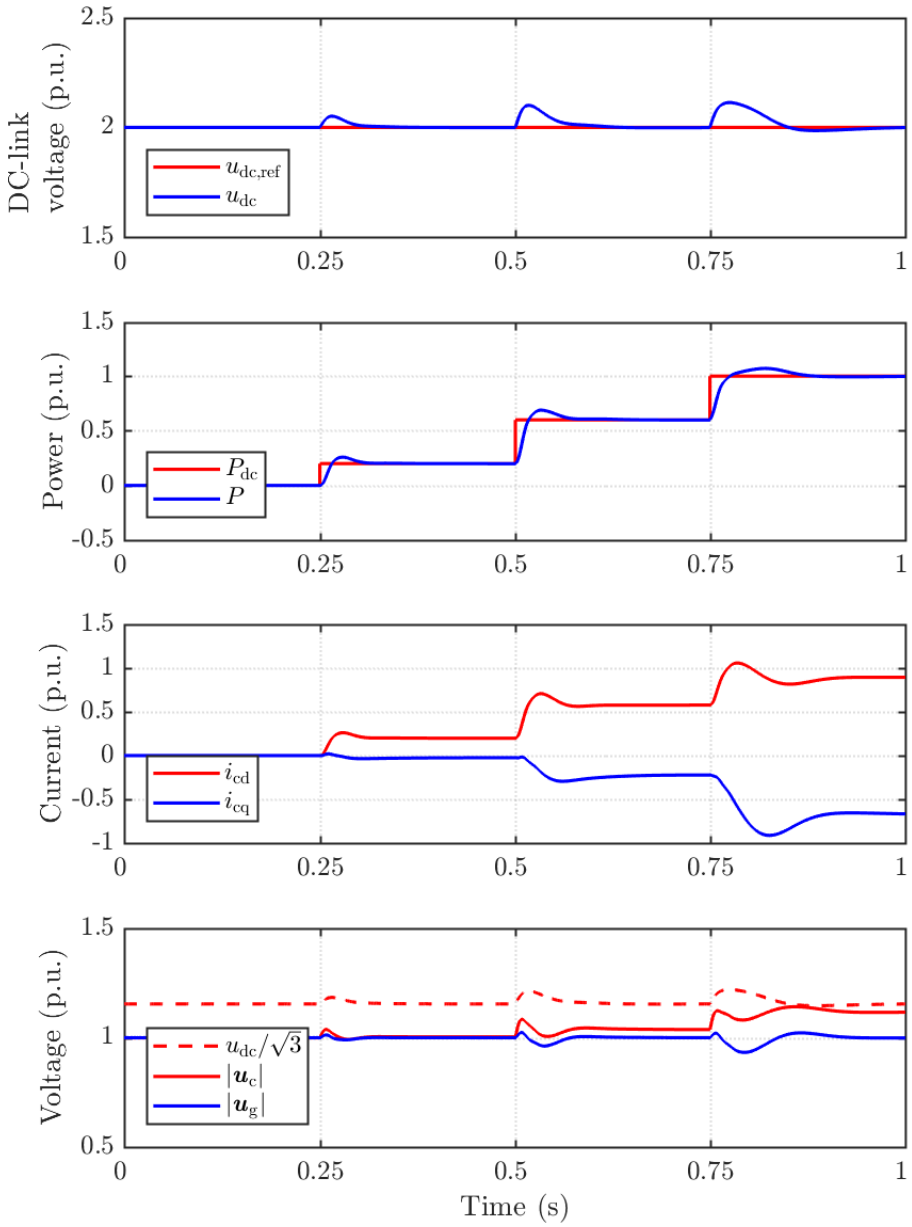

Figure 5.14: Step response of the modified vector control scheme 1 with the cascaded DC-link control for the weak grid.

Fig. 5.14 shows the step response with the cascaded DC-link controller for the weak grid. The scheme shows fast response at regulating the DC-link voltage to 2 p.u. Some low frequency oscillations are visible in the results which are due to the slow PLL bandwidth.

5.4 Modified Vector Control: Scheme 2

The simulation results of the scheme discussed in Section 3.5.2 are presented here. The parameters of the scheme 2 are same as scheme 1 and are listed in Table 5.4. The results are presented in Figs. 5.15 and 5.16 for the strong grid. The modified vector control scheme 2 works almost as good as the standard vector control scheme for strong-grid conditions (cf. Figs. 5.1 and 5.2). The response is also similar to scheme 1 for the strong grid.

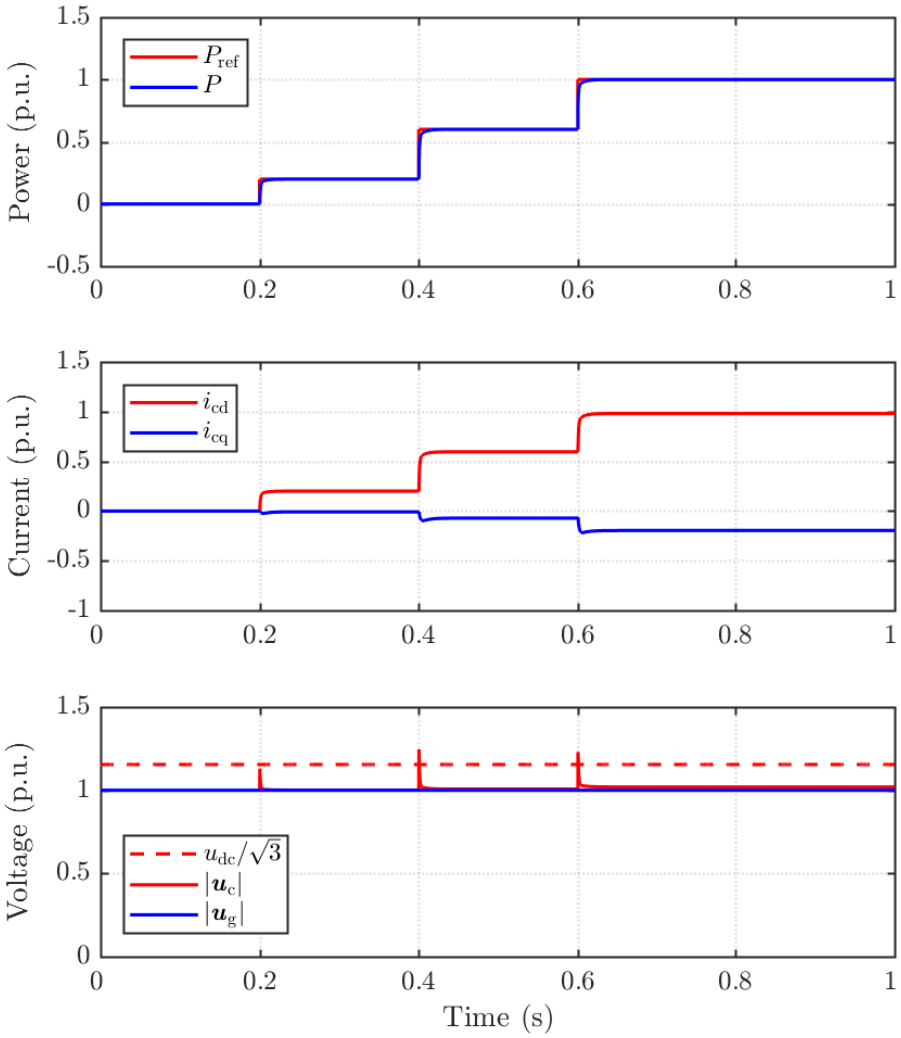

Figure 5.15: Step response of the modified vector control scheme 2 for the strong grid.

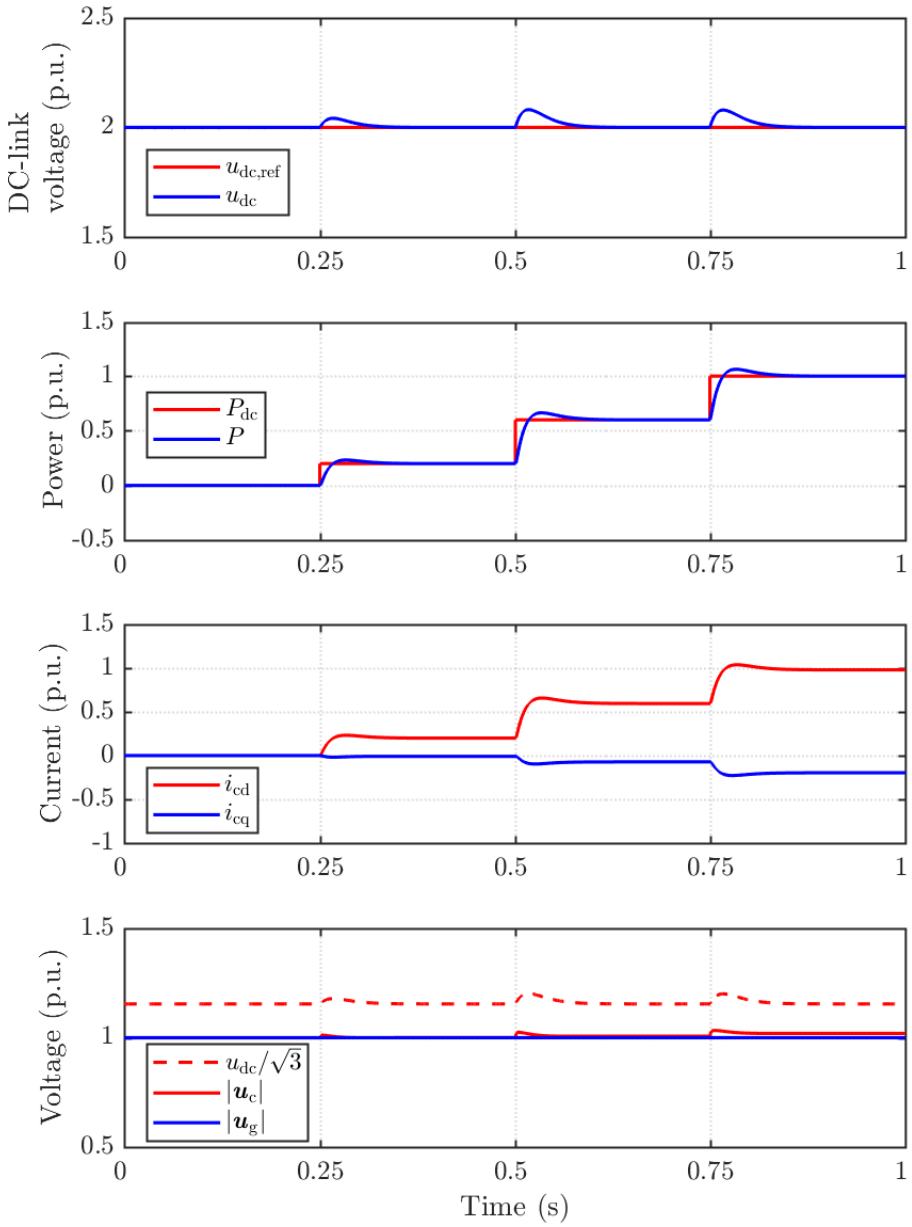

Figure 5.16: Step response of the modified vector control scheme 2 with the cascaded DC-link control for the strong grid.

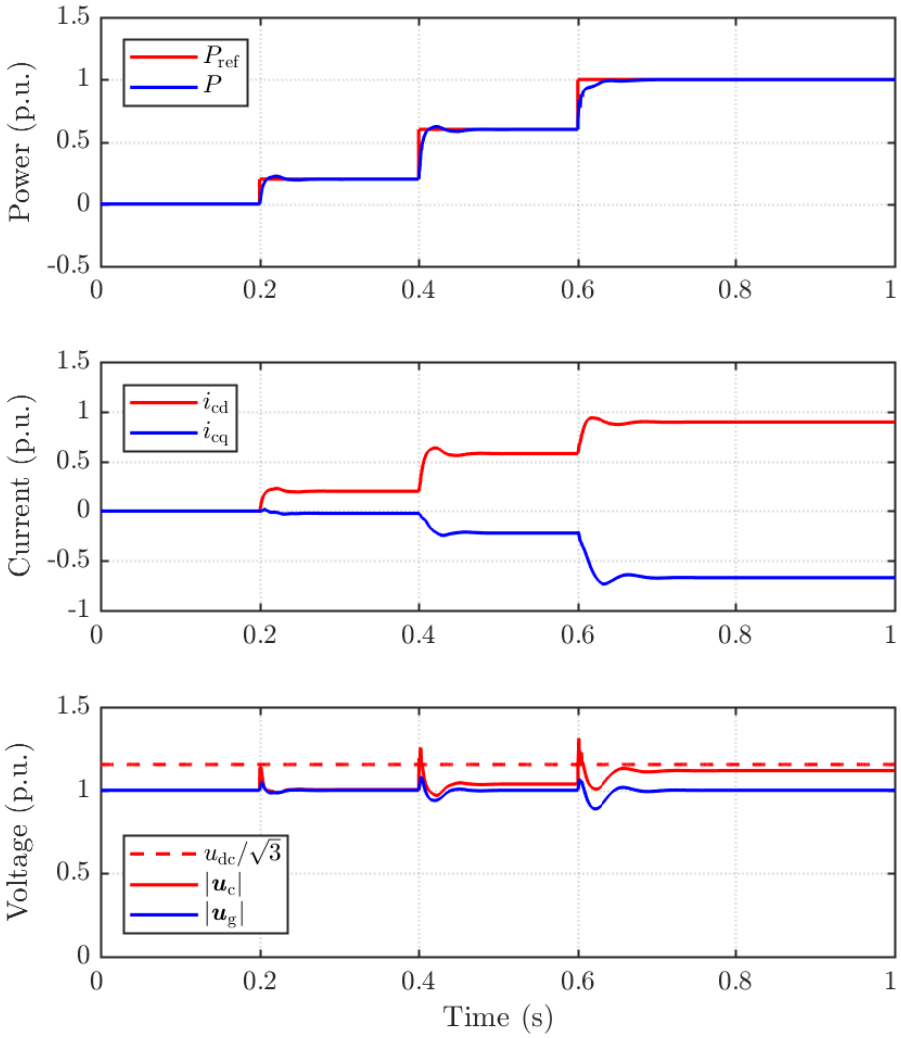

Figure 5.17: Step response of the modified vector control scheme 2 for the weak grid.

Fig. 5.17 shows the simulation results for the weak grid. The scheme provides good damping and the oscillations from the power are eliminated. The dynamic response is faster as compared to that of the scheme 1

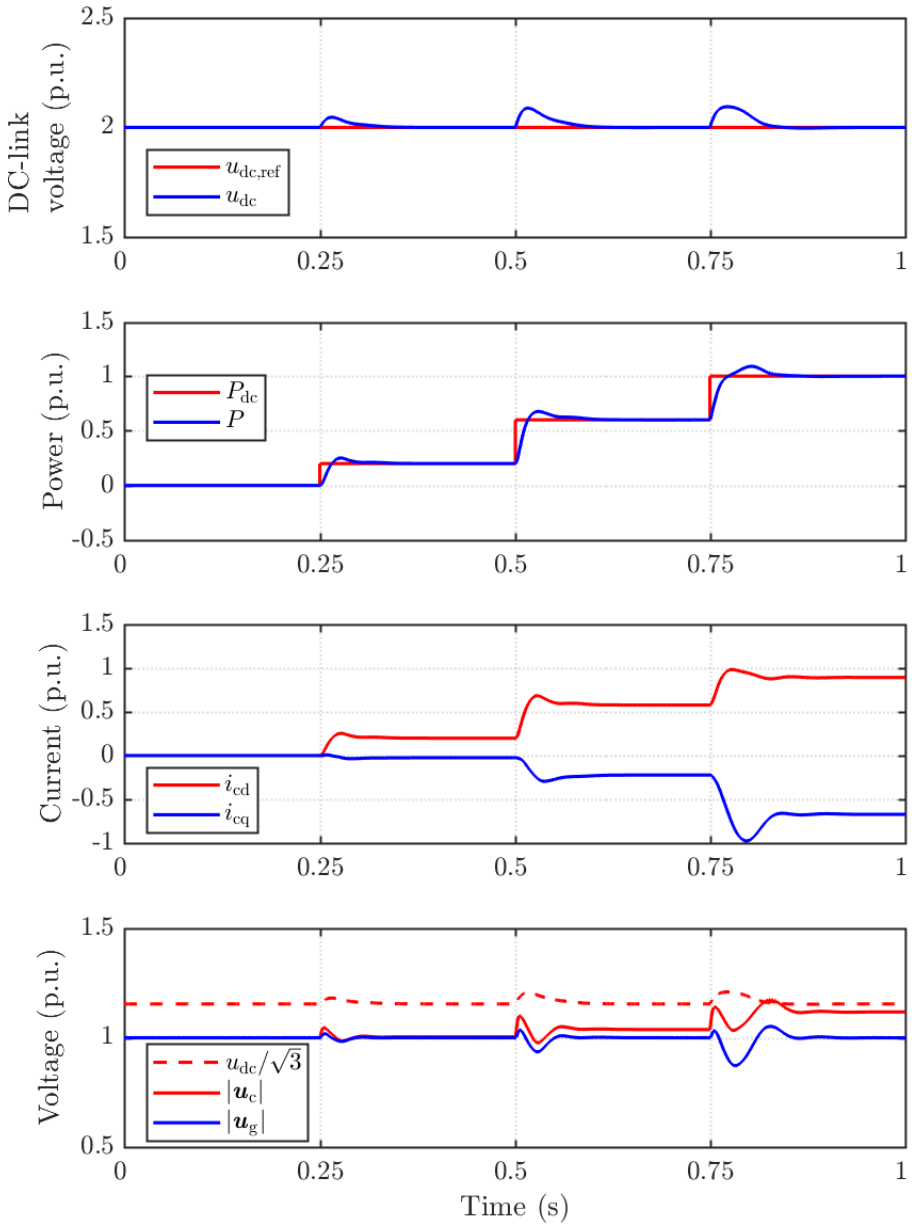

Figure 5.18: Step response of the modified vector control scheme 2 with the cascaded DC-link control for weak grids

Fig. 5.18 shows the simulation results for weak grids, when the scheme is cascaded with the DC-link controller. Low frequency oscillations in the PCC voltage are damped quickly as compared to those in scheme 1 (cf. Fig. 5.14).

5.5 PSC

The simulation results of the PSC scheme (cf. Fig. 3.7) are presented in this section. The control parameters are listed in Table 5.5. The step response of PSC for the strong grid is shown in Figs. 5.19 and 5.20. It has been identified in the literature that PSC does not work very well for strong grids as compared to standard vector control (cf. Fig. 5.1) and modified vector control (cf. Figs. 5.11 and 5.15) [25]. This is visible from the simulation results of PSC. There is a large overshoot and oscillations in the power flow. Also, there are some oscillations in the DC-link voltage when the DC-link voltage controller is used. It is also evident from the results that the modulator does not saturate during transients when PSC is used (cf. Fig. 5.19) as compared to the case when vector control is used (cf. Fig. 5.1). The reason is that the converter voltage magnitude is kept constant in PSC as discussed in Section 3.3.

Table 5.5: PSC Control Parameters

Parameter	Actual value	Normalized value
Active damping resistance R_{a}	2.2 Ω	0.2 p.u.
High-pass filter bandwidth ω_{b}	31 rad/s	0.1 p.u.
DC-link control gain k_{dc}	56 rad/s	0.18 p.u.
PLL gain k_{PLL}	2 rad/(V.s)	2 p.u.
AC-voltage controller integral gain	0.1 s^{-1}	-
AC-voltage controller proportional gain	50	-

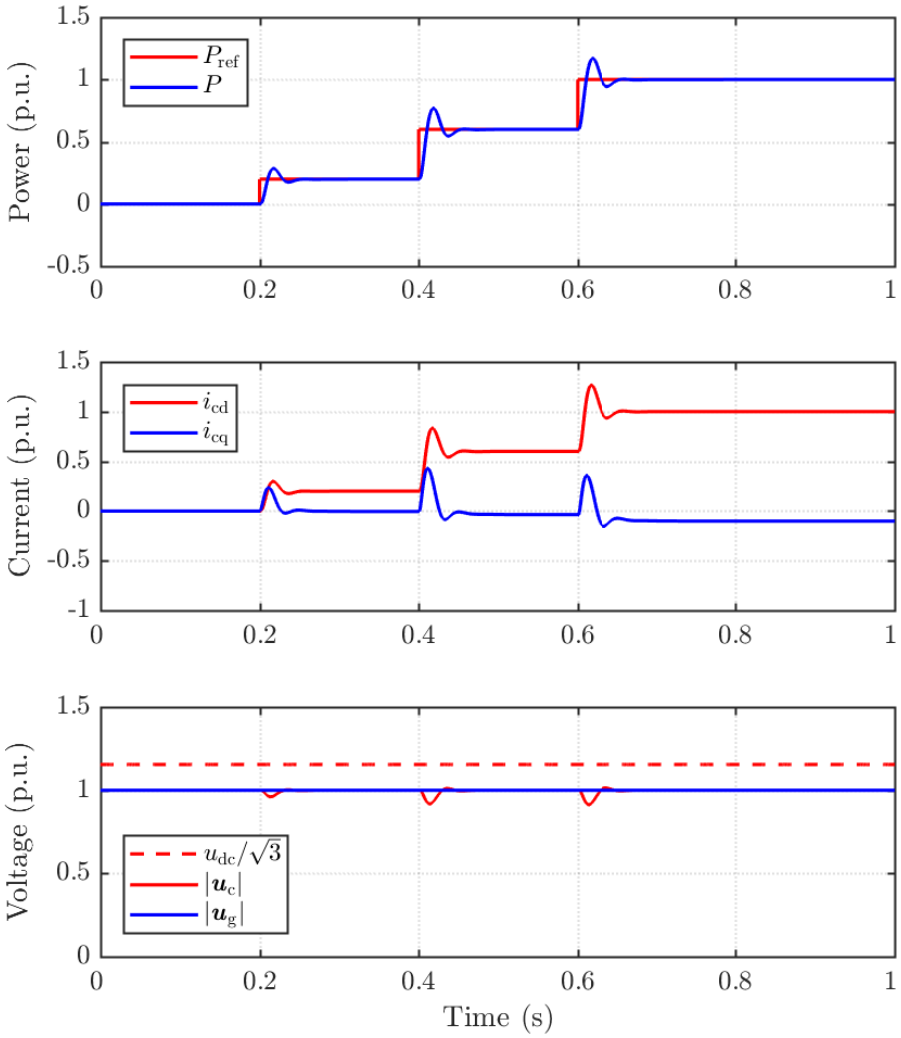

Figure 5.19: Step response of PSC for the strong grid.

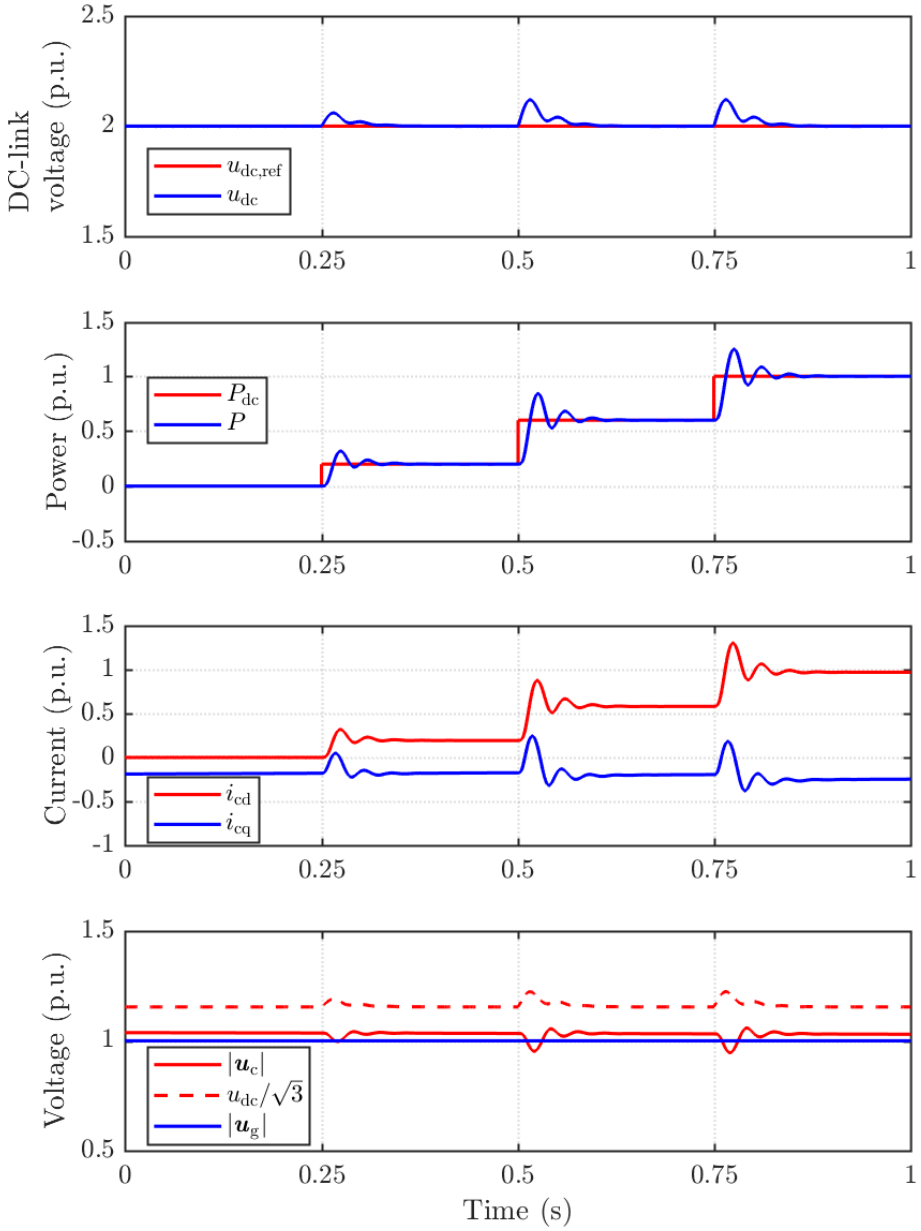

Figure 5.20: Step response of PSC with cascaded DC-link control for the strong grid.

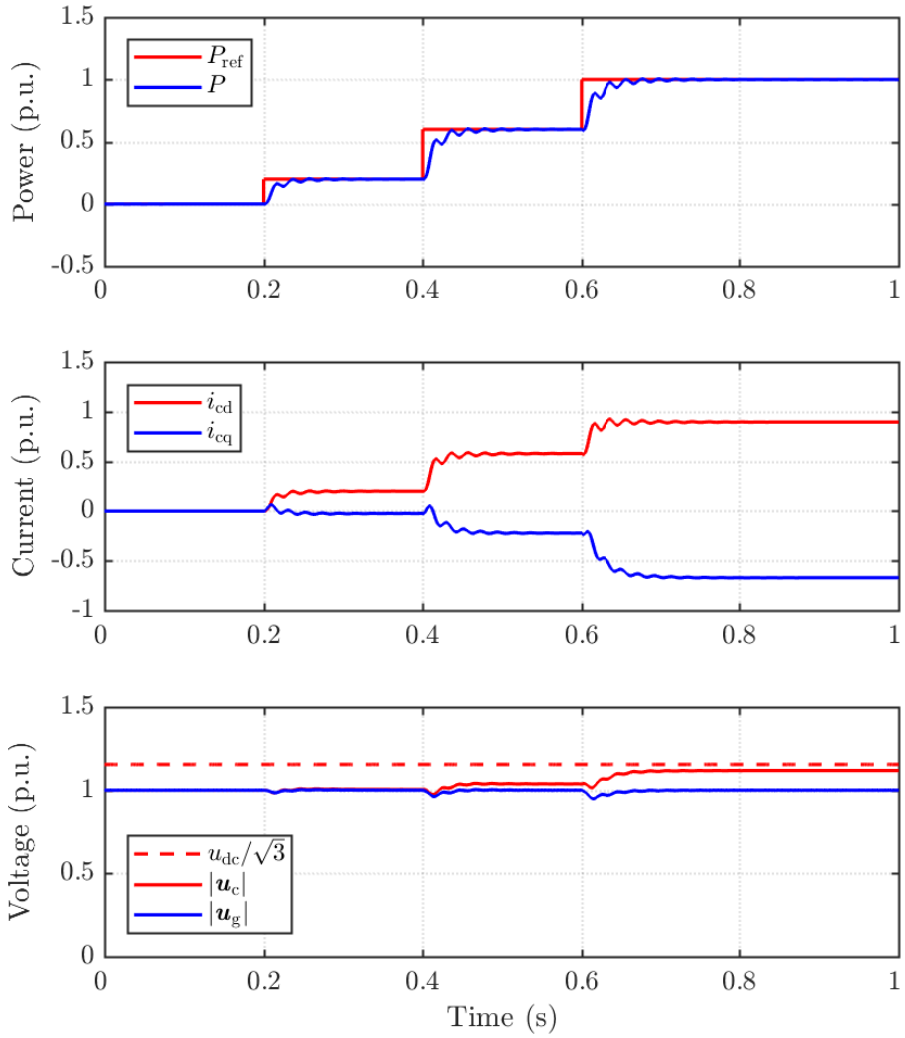

Figure 5.21: Step response of PSC for the weak grid.

Fig. 5.21 shows the power step response of PSC for the weak grid. At 0.6 s instant, the response seems to have a non-minimum phase behavior which means that the power is undershooting or decreasing before increasing. Also, there are ripples in the power flow which are not present when the modified vector control schemes are used (cf. Figs. 5.13 and 5.17).

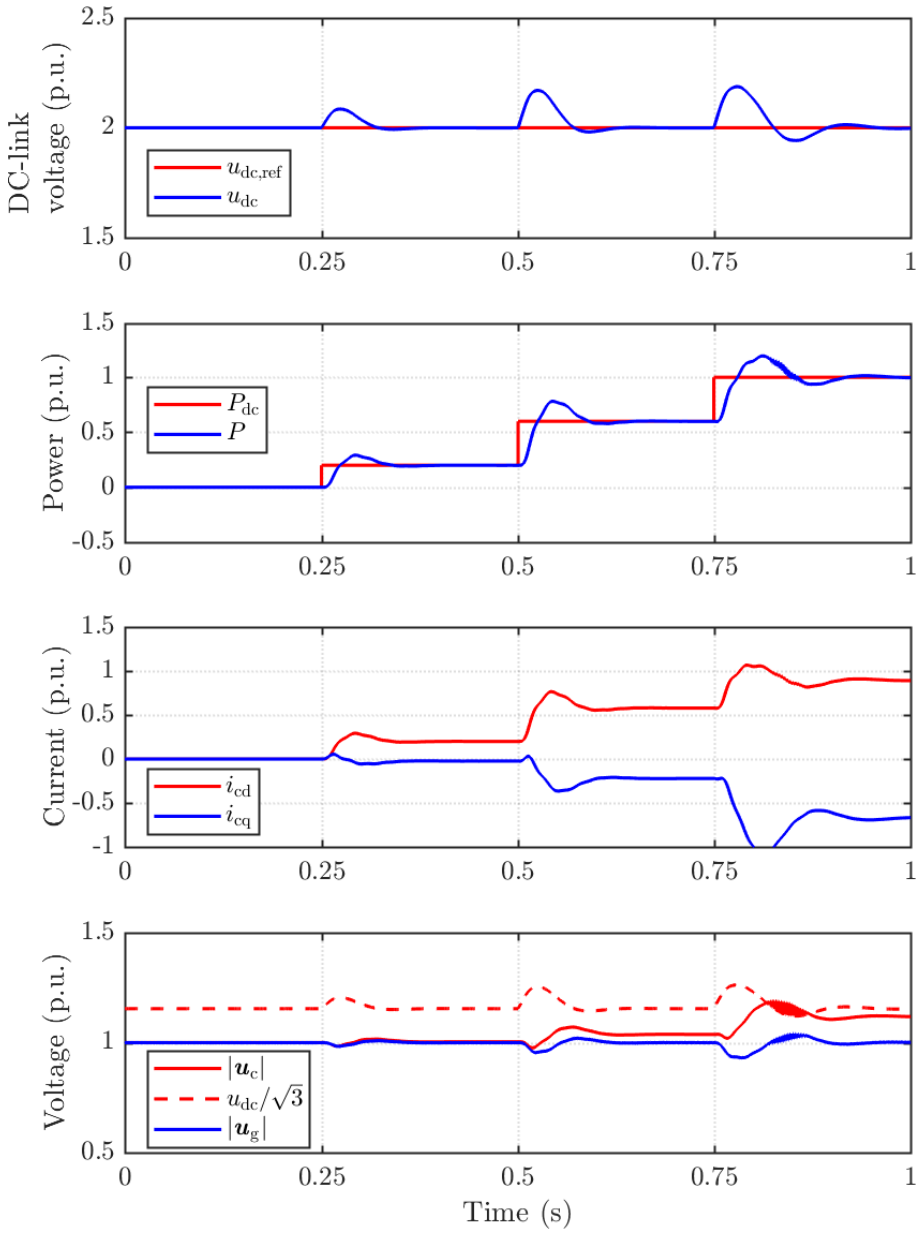

Figure 5.22: Step response of PSC with cascaded DC-link control for the weak grid.

Fig. 5.22 shows the simulation results with the cascaded DC-link controller. The scheme is able to regulate the DC-link voltage at 2 p.u. with some oscillations. The scheme is stable under weak-grid conditions unlike the standard vector control scheme (cf. Fig. 5.4). In comparison to the modified vector control schemes, the PSC has larger deviations in the DC-link voltage during transients and slower response. Also, the modulator is saturating which is not the case for the modified vector control schemes (cf. Figs. 5.14 and 5.18).

6 Conclusion

In this thesis, the performance of converter control schemes is studied with the focus on weak-grid conditions. Two state-of-the-art control schemes (Vector control and PSC) are considered as a starting point. An L filter is used to suppress the converter harmonics. The working and control structure of these schemes have been explained in detail. A standard vector-controlled converter is unable to transfer its maximum theoretical power of 1 p.u., when connected to a weak grid. In addition, the power quality is also compromised. The root causes of the problem have been mentioned in this thesis and the solutions have been suggested. Two novel modified vector control schemes have been presented for an improved operation under weak-grid conditions. Vector diagrams are used to illustrate the steady state operation. Time domain simulations have been used to compare the performance of the control schemes.

In order to transfer 1 p.u. of power in weak grids, an AC-voltage controller is necessary. In addition, the bandwidth of the PLL needs to be reduced in order to make it less sensitive to the changes in the PCC voltage. Vector control is augmented with an outer-loop power controller. The active-power controller is tuned to have slow closed-loop dynamics as compared to the AC-voltage control loop. The response of the vector control scheme improves and the oscillations from the power are eliminated. The downside of using this scheme is that the response becomes very slow also for strong grids.

Two novel modified vector control schemes have also been suggested. The first scheme consists of a high-pass filtered converter voltage reference magnitude feed-back which is subtracted from the power reference. The resulting system shows fast response but the low frequency oscillations can be seen in the PCC voltage when a cascaded DC-link controller is used. The second scheme uses high-pass filtered real and imaginary components of the converter voltage reference as a feed-back to modify active and reactive power references. The scheme good damping and fast dynamic response under all grid strengths and the low frequency oscillations in the PCC voltage are also damped better.

Finally, the operation of PSC is also tested using simulations and compared with the modified vector control scheme. PSC shows stable and smooth response for weak

grids but its performance is compromised for strong grids. The step response for strong grids shows overshoot and oscillations.

Based on the above findings, it can be concluded that the modified vector control scheme can be used to control a VSC irrespective of the grid strength. It has a clear advantage over PSC that it can limit over currents in case of short circuits due to an inner current controller. Also, the performance of the system is not compromised when connected to a strong grid.

Future work can include the comparison of these schemes based on the analytical models. A linearized model can be used to get the better understanding of operation in weak grids. The proposed modified vector control schemes will be tested with an LCL filter. Alternative methods of filtering out the PWM ripple from the PCC voltage measurement can be developed. The schemes will be tested in the lab.

References

[1] P. Pinson, L. Mitridati, C. Ordoudis, and J. Ostergaard, "Towards fully renewable energy systems: Experience and trends in Denmark," *CSEE Journal of Power and Energy Systems*, vol. 3, no. 1, pp. 26–35, March 2017.

[2] M. I. Marei, E. F. El-Saadany, and M. M. A. Salama, "Flexible distributed generation:(FDG)," in *IEEE Power Engineering Society Summer Meeting*, vol. 1, July 2002, pp. 49–53.

[3] Y. Huang, X. Yuan, J. Hu, P. Zhou, and D. Wang, "DC-bus voltage control stability affected by AC-bus voltage control in VSCs connected to weak AC grids," *IEEE Journal of Emerging and Selected Topics in Power Electronics*, vol. 4, pp. 445–458, June 2016.

[4] Y. Huang, X. Yuan, and J. Hu, "Effect of reactive power control on stability of DC-link voltage control in VSC connected to weak grid," in *IEEE PES General Meeting | Conference Exposition*, July 2014, pp. 1–5.

[5] "IEEE guide for planning DC links terminating at AC locations having low short-circuit capacities," *IEEE Std. 1204-1997*, pp. 1–216, Jan. 1997.

[6] B. T. Ooi and X. Wang, "Voltage angle lock loop control of the boost type PWM converter for HVDC application," *IEEE Transactions on Power Electronics*, vol. 5, no. 2, pp. 229–235, Apr. 1990.

[7] M. Lindgren, "Modeling and control of voltage source converters connected to the grid," Ph.D. dissertation, Chalmers University of Technology, Göteborg, Sweden, 1998.

[8] P. Zhou, X. Yuan, J. Hu, and Y. Huang, "Stability of DC-link voltage as affected by phase locked loop in VSC when attached to weak grid," in *IEEE PES General Meeting | Conference Exposition*, July 2014, pp. 1–5.

[9] M. Durrant, H. Werner, and K. Abbott, "Model of a VSC HVDC terminal attached to a weak AC system," in *Proceedings of IEEE Conference on Control Applications*, vol. 1, June 2003, pp. 178–182.

[10] Q. C. Zhong, P. L. Nguyen, Z. Ma, and W. Sheng, "Self-synchronized synchronverters: Inverters without a dedicated synchronization unit," *IEEE Transactions on Power Electronics*, vol. 29, no. 2, pp. 617–630, Feb. 2014.

[11] L. Zhang, L. Harnefors, and H. P. Nee, "Power-synchronization control of grid-connected voltage-source converters," *IEEE Transactions on Power Systems*, vol. 25, no. 2, pp. 809–820, May 2010.

[12] W. Zhang, A. M. Cantarellas, J. Rocabert, A. Luna, and P. Rodriguez, "Synchronous power controller with flexible droop characteristics for renewable

power generation systems," *IEEE Transactions on Sustainable Energy*, vol. 7, no. 4, pp. 1572–1582, Oct. 2016.

[13] L. Zhang, "Modeling and control of VSC-HVDC links connected to weak AC systems," Ph.D. dissertation, KTH, School of Electrical Engineering, Stockholm, Sweden, 2010.

[14] L. Zhang, L. Harnefors, and H. P. Nee, "Interconnection of two very weak AC systems by VSC-HVDC links using power-synchronization control," *IEEE Transactions on Power Systems*, vol. 26, no. 1, pp. 344–355, Feb. 2011.

[15] P. Mitra, L. Zhang, and L. Harnefors, "Offshore wind integration to a weak grid by VSC-HVDC links using power-synchronization control: A case study," *IEEE Transactions on Power Delivery*, vol. 29, no. 1, pp. 453–461, Feb. 2014.

[16] "IEEE recommended practice and requirements for harmonic control in electric power systems," *IEEE Std. 519-2014*, pp. 1–213, June 2014.

[17] H. P. Beck and R. Hesse, "Virtual synchronous machine," in *9th International Conference on Electrical Power Quality and Utilisation*, Oct. 2007, pp. 1–6.

[18] Q. C. Zhong and G. Weiss, "Synchronverters: Inverters that mimic synchronous generators," *IEEE Transactions on Industrial Electronics*, vol. 58, no. 4, pp. 1259–1267, April 2011.

[19] M. Lindgren and J. Svensson, "Control of a voltage-source converter connected to the grid through an LCL-filter-application to active filtering," in *29th Annual IEEE Power Electronics Specialists Conference*, vol. 1, May 1998, pp. 229–235.

[20] H. Akagi, Y. Kanazawa, and A. Nabae, "Instantaneous reactive power compensators comprising switching devices without energy storage components," *IEEE Transactions on Industry Applications*, vol. IA-20, no. 3, pp. 625–630, May 1984.

[21] V. Kaura and V. Blasko, "Operation of a phase locked loop system under distorted utility conditions," *IEEE Transactions on Industry Applications*, vol. 33, no. 1, pp. 58–63, Jan. 1997.

[22] J. Z. Zhou and A. M. Gole, "VSC transmission limitations imposed by AC system strength and AC impedance characteristics," in *10th IET International Conference on AC and DC Power Transmission*, Dec. 2012, pp. 1–6.

[23] S. H. Huang, J. Schmall, J. Conto, J. Adams, Y. Zhang, and C. Carter, "Voltage control challenges on weak grids with high penetration of wind generation: Ercot experience," in *IEEE Power and Energy Society General Meeting*, July 2012, pp. 1–7.

[24] M. F. M. Arani and Y. A. R. I. Mohamed, "Analysis and performance enhancement of vector-controlled VSC in HVDC links connected to very weak grids," *IEEE Transactions on Power Systems*, vol. 32, no. 1, pp. 684–693, Jan. 2017.

[25] L. Harnefors, M. Hinkkanen, F. M. M. Rahman, U. Riaz, and L. Zhang, "Robust design of power-synchronization control," - to be published.

[26] S. I. Nanou and S. A. Papathanassiou, "Grid code compatibility of VSC-HVDC connected offshore wind turbines employing power synchronization control," *IEEE Transactions on Power Systems*, vol. 31, no. 6, pp. 5042–5050, Nov. 2016.

[27] G. Wu, J. Liang, X. Zhou, Y. Li, A. Egea-Alvarez, G. Li, H. Peng, and X. Zhang, "Analysis and design of vector control for VSC-HVDC connected to weak grids," *CSEE Journal of Power and Energy Systems*, vol. 3, no. 2, pp. 115–124, June 2017.

[28] A. Egea-Alvarez, S. Fekriasl, F. Hassan, and O. Gomis-Bellmunt, "Advanced vector control for voltage source converters connected to weak grids," *IEEE Transactions on Power Systems*, vol. 30, no. 6, pp. 3072–3081, Nov. 2015.

[29] L. Harnefors and H. P. Nee, "Model-based current control of AC machines using the internal model control method," *IEEE Transactions on Industry Applications*, vol. 34, no. 1, pp. 133–141, Jan. 1998.